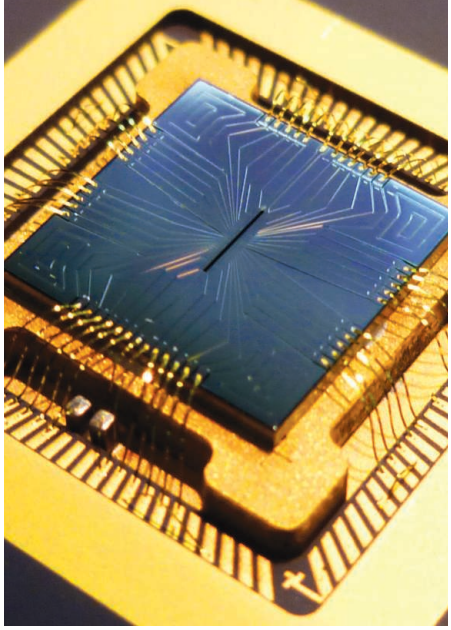

PHOTO: CURT SUPLEE AND EMILY EDWARDS, JOINT QUANTUM INSTITUTE AND UNIVERSITY OF MARYLAND; CHIP FABRICATION: SANDIA NATIONAL LABORATORIES WITH SUPPORT FROM THE INTELLIGENCE ADVANCED RESEARCH PROJECTS ACTIVITY

INTRODUCTION

The Future of Quantum Information Processing

IN A WORLD OVERWHELMED BY INCREASING AMOUNTS OF DATA, FINDING NEW WAYS to store and process information has become a necessity. Conventional silicon-based electronics has experienced rapid and steady growth, thanks to the progressive miniaturization of its basic component, the transistor, but that trend cannot continue indefinitely.

In conventional devices, information is stored and manipulated in binary form: The elementary components of these devices—the so-called bits—have two states, each of which encodes the binary 0 or 1. To move beyond the binary system, one can exploit the laws of quantum mechanics. A quantum-mechanical object with two energy levels at its disposal can occupy either of those two levels, but also an arbitrary combination ("superposition") of the two, much like an electron in a two-slit experiment can go through both slits at once. This results in infinitely many quantum states that a single quantum bit, or "qubit," can take; together with another strange property of quantum mechanics—entanglement—it allows for a much more powerful information platform than is possible with conventional components.

Quantum information processing (QIP) uses qubits as its basic information units. QIP has many facets, from quantum simulation, to cryptography, to quantum computation, which is expected to solve problems more complex than those within the capabilities of conventional computers. To be useful for QIP, a qubit needs to be both isolated from its environment and tightly controllable, which places stringent requirements on its physical realization. But this is only the first step; to build a quantum computer, for example, we must also have a scalable architecture and error correction that can be performed in parallel with computation; in addition, efficient quantum algorithms must exist for solving the problem at hand—a considerable theoretical challenge.

A number of qubit types have been proposed and experimentally realized that satisfy at least some of these criteria, and tremendous progress has been made over the past decade in improving the figures of merit, such as the coherence time. In this special section, four Reviews look into the future of QIP in some of its most promising physical realizations. On p. 1164, Monroe and Kim discuss the challenges of scaling trapped ion architectures to hundreds and thousands of qubits and beyond. Devoret and Schoelkopf (p. 1169) speculate on the future of superconducting circuits, whereas Awschalom *et al.* (p. 1174) focus on the many promising qubit flavors based on spins in semiconductors. Finally, Stern and Lindner (p. 1179) lay out the prospects for quantum computation using the entirely different approach of topologically protected states.

The future of QIP appears bright in spite of the many remaining challenges. As a bonus, overcoming these challenges will probably also advance basic research.

– JELENA STAJIC

Online

sciencemag.org

Podcast interview with author D. D. Awschalom (http://scim.ag/pod_6124a).

Quantum Information Processing

CONTENTS

Reviews

See also Science *Podcast*

Science

Published by AAAS

REVIEW

Scaling the Ion Trap Quantum Processor

C. Monroe[1]* and J. Kim[2,3]

Trapped atomic ions are standards for quantum information processing, serving as quantum memories, hosts of quantum gates in quantum computers and simulators, and nodes of quantum communication networks. Quantum bits based on trapped ions enjoy a rare combination of attributes: They have exquisite coherence properties, they can be prepared and measured with nearly 100% efficiency, and they are readily entangled with each other through the Coulomb interaction or remote photonic interconnects. The outstanding challenge is the scaling of trapped ions to hundreds or thousands of qubits and beyond, at which scale quantum processors can outperform their classical counterparts in certain applications. We review the latest progress and prospects in that effort, with the promise of advanced architectures and new technologies, such as microfabricated ion traps and integrated photonics.

Quantum physics can be distilled to two disjointed and counterintuitive rules. First, an isolated quantum system is represented by a "wave function," or a mathematical entity that evolves according to a wave equation and is shaped with external controls. Second, when a quantum system interacts with a measurement apparatus or its surrounding environment, the wave function probabilistically and irreversibly "collapses" into a particular state. The incompatibility of these two quantum rules is seen most clearly in a quantum superposition state, in which, for instance, an isolated particle's wave function is delocalized between two or more positions. The second rule ensures that such states are never directly seen in the macroscopic world. However, when a system is left isolated without interacting with its environment, the (microscopic) superposition persists and can be exploited to store massive amounts of information in parallel.

A quantum information processor encodes information in an array of quantum bits or qubits, which can hold superpositions of classical bit values 0 and 1. When N qubits are prepared in their most general state, we have a quantum superposition of all 2^N N-bit binary numbers. Such a superposition is typically "entangled" in the sense that certain qubit values are correlated with others, even though they yield random outcomes when measured individually. A quantum computer manipulates this exponential amount of information by interfering pieces of this complex superposition through controlled interactions, or quantum logic gate operations. A final measurement of the system can then yield information pertaining to all 2^N states. For merely $N = 400$ qubits, we find that the encoded information of $2^{400} \sim 10^{120}$ values is more than the number of fundamental particles in the universe; such a computation could never be performed without the parallel processing enabled by quantum mechanics. In a sense, entanglement between qubits acts as an invisible wiring that can potentially be exploited to solve certain problems that are intractable otherwise (*1*).

The requirements for large-scale quantum computer hardware are daunting, given the exponential sensitivity of such large superpositions to errors and leaks to the environment. However, there exist error-correction codes that allow arbitrarily complex quantum superposition states to be generated and stabilized (*1*), giving us hope that useful fault-tolerant quantum computers will eventually be realized despite the steep technical requirements far beyond current experimental capability.

In the search for quantum information processing hardware, one needs qubits that are extremely well isolated from the environment yet can be precisely controlled with external fields to affect interferences through the operations of quantum logic gates. Moreover, we must ultimately couple the qubits to the outside world in the strongest possible sense by performing a measurement that collapses any superposition onto definite values. These conflicting stringent requirements restrict potential quantum hardware to exotic microscopic systems. In this Review, we consider the most fundamental of these platforms—electromagnetically trapped atoms (*2*)—and speculate how this system may be scaled to hundreds or thousands of interacting qubits in the coming years.

Entangling Trapped Atomic Ion Qubits

Individual atoms are natural carriers of quantum information because they are standards: An isolated atom of carbon, for example, is exactly the same in Washington as it is in London or anywhere else. Isolation can be provided by confining atoms in an evacuated environment with electromagnetic traps, suspending atoms in free space so that they do not uncontrollably interact with background atoms, molecules, or surfaces. There are several compelling proposals for quantum computer architectures based on trapped neutral atoms and optical lattices, although the weak interaction between neutral atoms leads to difficulties in controlling their entanglement, and research in this area is still exploratory (*3*). Here, we focus on the trapping of electrically charged atoms, or ions, for which high-fidelity quantum operations and measurements are now commonplace.

The typical ion trap geometry for quantum information purposes is the linear radio frequency (rf) Paul trap, in which nearby electrodes hold static and dynamic electrical potentials that lead to an effective harmonic confinement of the ions, like a bowl full of mutually repelling marbles (*2*). When ions are laser-cooled to very low temperatures in such a trap, the ions form a linear crystal of qubits, with the Coulomb repulsion balancing the external confinement force (Fig. 1A). Ions are typically loaded into traps by creating a neutral atomic flux of the desired particle and ionizing them once in the trapping volume. Ions can remain confined for months, with lifetimes often limited by the level of vacuum. Elastic collisions with residual background gas occur roughly once per hour per ion at typical ultrahigh-vacuum pressures ($\sim 10^{-11}$ torr) and do not necessarily eject the ion, although inelastic collisions can change the species of the trapped ion. Cryogenic chambers can virtually eliminate these collision events by further reducing the background pressure.

Appropriate atomic ion species should have a strong closed optical transition that allows for laser-cooling of the motion, qubit state initialization, and efficient qubit readout. This rules out almost anything other than simple atomic ions with a lone outer electron, such as the alkaline-earths (Be^+, Mg^+, Ca^+, Sr^+, and Ba^+) and particular transition metals (Zn^+, Hg^+, Cd^+, and Yb^+). Qubits are represented by two stable electronic levels within each ion, sometimes characterized by an effective spin with the two states $|\uparrow\rangle$ and $|\downarrow\rangle$ corresponding to bit values 0 and 1.

The reduced energy level diagram of $^{171}Yb^+$ is shown in Fig. 2, B and C, in which the qubit levels $|\uparrow\rangle$ and $|\downarrow\rangle$ are represented by the stable hyperfine levels in the ground electronic state, separated by frequency $\nu_{HF} = 12.642\ 812$ GHz. The excited electronic states $|e\rangle$ and $|e'\rangle$ are themselves split by a smaller hyperfine coupling and separated from the ground states by an optical interval. Laser radiation tuned just below resonance in these optical transitions allows Doppler laser cooling to confine ions near the bottom of the trap. Other more sophisticated forms of laser cooling can bring the ions to nearly at rest in the trap (*4*). When a bichromatic laser beam resonant with both $|\uparrow\rangle \leftrightarrow |e\rangle$ and $|\uparrow\rangle \leftrightarrow |e'\rangle$ transitions is applied to the atom, it rapidly falls into the state $|\downarrow\rangle$ and no longer interacts with the light

[1]Joint Quantum Institute (JQI), Department of Physics, University of Maryland, and National Institute of Standards and Technology, College Park, MD 20742, USA. [2]Department of Electrical and Computer Engineering, Duke University, Durham, NC 27708, USA. [3]Applied Quantum Technologies, Durham, NC 27707, USA.

*To whom correspondence should be addressed. E-mail: monroe@umd.edu

field (Fig. 1B), allowing the initialization of a qubit with essentially 100% fidelity. When a single laser resonant with the transition $|\uparrow\rangle \leftrightarrow |e\rangle$ is applied, the closed-cycling optical transition causes an ion in the $|\uparrow\rangle$ state to fluoresce strongly, whereas an ion in the $|\downarrow\rangle$ state stays dark because the laser is far from its resonance (Fig. 1C). The collection of even a small fraction of this fluoresence allows for the detection of the atomic qubit state with near-perfect efficiency. Other atomic species have similar initialization/detection schemes.

Coulomb-Based Gates and the Quantum CCD

The motion of many trapped ions is coupled through the Coulomb interaction, much like an array of pendulums connected by springs. A natural way to implement entangling quantum logic gates between ions in a crystal is thus to use the motion as an intermediary (Fig. 2A) by applying qubit state–dependent optical or microwave dipole forces to the ion (or ions) (*4*–*7*).

We assume that the qubit levels respond to an external field E by experiencing an equal and opposite energy shift $\pm\mu E$—for example, through the Stark effect for electric fields or the Zeeman effect for magnetic fields, in which case μ is an effective dipole moment of the qubit. When the field is inhomogeneous, this gives rise to a qubit state–dependent force along the x direction $F_x = \pm\mu E'(x)$, where the sign depends on the qubit state, and $E'(x)$ is the gradient of the applied field along x. For a plane wave radiation field with amplitude E_0 and wave vector k along x, $F_x = \pm\hbar k\Omega$, where h is Planck's constant, and the Rabi frequency $\Omega = \mu E_0/h$ parametrizes the field-qubit coupling. Because this force acts differently on the two qubit states, it can coherently map the qubit state to the collective motion of N ions, with characteristic speed $R_{gate} = \Omega\sqrt{\nu_R/\nu}$ (*4*, *7*). In this expression, $\nu_R = \hbar k^2/(8\pi^2 M)$ is the recoil frequency of the ion crystal associated with momentum transfer from the field, M is the total mass of the ions, and ν is the frequency of harmonic oscillation of the collective motional mode along the x direction. Thus, a qubit superposition within the ion is transformed to a superposition of the ion's position. When applied to multiple ions, this fundamental operation allows gates to be performed between separated ions, mediated through the motion (*5*, *6*). Current experiments with a few ions have realized entangled state fidelities of greater than 99% (*8*) and operate in the range $R_{gate} \sim 10$ to 100 kHz; with available ultrafast optical fields, it should be possible to operate gates in the gigahertz range (*9*).

As the number of ions N in the crystal grows, the gate speed slows down as $R_{gate} \sim 1/\sqrt{N}$ from the mass term. For large crystals, there will also be crosstalk between the many modes of collective motion. Background errors such as the decoherence (heating) of the motional modes (*10*) or fluctuating fields that add random phases to the qubits will become important at longer times; thus, there will be practical limits on the size of a single crystal for the performance of faithful quantum gates. Individual optical addressing of ions (*11*) and pulse-shaping techniques (*12*) can mitigate these errors to achieve the full control of single crystals ranging from $N = 10$ to 100 qubits. This should allow the implementation of quantum simulations (*13*) in a regime in which classical modeling of certain many-body systems, such as frustrated spin networks, becomes intractable. It would also enable the construction of error-correcting encoded qubits that might form block primitives of an eventual fault-tolerant quantum computer.

In order to scale beyond 10 to 100 trapped ion qubits, we turn to a multiplexed architecture called the quantum charge-coupled device (QCCD) (*14*). This involves the sequential entanglement of small numbers of ions through their collective motion in a single chain and the classical shuttling of individual ions between different trapping zones to propagate the entanglement, as depicted in Fig. 2B. The QCCD architecture requires exquisite control of the ion positions during shuttling and may require additional atomic ion species to act as "refrigerator" ions to quench the excess motion from shuttling operations (*15*). Rudimentary versions of the QCCD idea have been used in many quantum information applications, such as teleportation and small quantum algorithms (*7*), and recent experiments have shown the reliable, repeatable, and coherent shuttling of ion qubits over millimeter distances in microseconds (*16*, *17*) and through complex two-dimensional junctions (Fig. 2, C and D) (*18*, *19*). The QCCD approach will push current state-of-the-art quantum information processing experiments to territories where elementary quantum error correction and simple quantum algorithms can be implemented. However, scaling to thousands or more qubits in the QCCD may be challenging because of the complexity of interconnects, diffraction of optical beams, and the extensive hardware required for qubit control.

Photonic Gates and Joining Remote Crystals

To scale beyond the QCCD in a modular architecture, one can link separate registers of trapped ion chains with photonic interfaces. In this scheme, an entangled qubit pair is first generated between the two registers, which is then used to implement a two-qubit gate between two ions that belong to each register (*20*). This approach is not limited to trapped ions and can be generalized to other physical systems with strong optical transitions (*3*).

A pair of trapped ion qubit registers [termed elementary logic units (ELUs)] can be entangled with each other by using propagating photons emitted by a subset of ions from each register, designated to be "communication qubits." Each communication qubit is driven to an excited state with near unit probability $p_e \sim 1$ by using a fast laser pulse, so that at most one photon emerges following appropriate radiative selection rules (Fig. 2E). The photon carries its qubit through two distinguishable internal photonic states (such as polarization or optical frequency) (*21*, *22*). For example, the joint state of a communication qubit and emitted photonic qubit can be written $|\downarrow\rangle_i|\nu_\downarrow\rangle_i + |\uparrow\rangle_i|\nu_\uparrow\rangle_i$, where $|\nu_\downarrow\rangle_i$ and $|\nu_\uparrow\rangle_i$ denote the frequency qubit states of a single photon

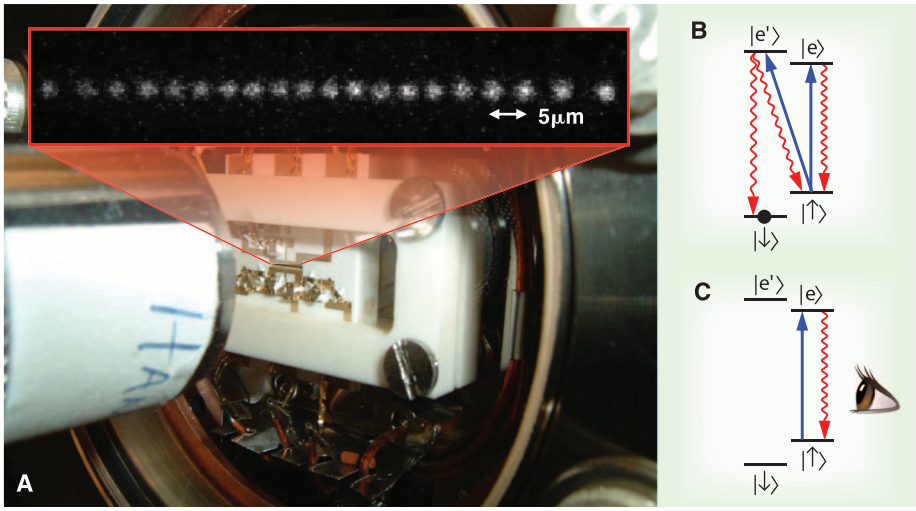

Fig. 1. (**A**) Vacuum chamber that houses electrodes for the trapping of atomic ions with a linear crystal of 20 confined atomic $^{171}Yb^+$ ions laser cooled to be nearly at rest. The atoms are illuminated with laser radiation tuned to a resonance in $^{171}Yb^+$, and the fluorescence is imaged onto a camera. The separation of the ions is determined by a balance between the external confinement force and Coulomb repulsion. (**B** and **C**) Reduced energy level diagram of each $^{171}Yb^+$ atomic ion, showing the atomic hyperfine levels $|\uparrow\rangle$ and $|\downarrow\rangle$ that represent a qubit. The electronic excited states $|e\rangle$ and $|e'\rangle$ are separated from the ground states by an energy corresponding to an optical wavelength of 369.53 nm, with all allowed transitions indicated by the downward red arrows. Applied laser radiation (upward blue arrows) drives these transitions for (B) initialization to state $|\downarrow\rangle$ and (C) fluorescence detection of the qubit state ($|\uparrow\rangle$, fluorescence, $|\downarrow\rangle$, no fluorescence).

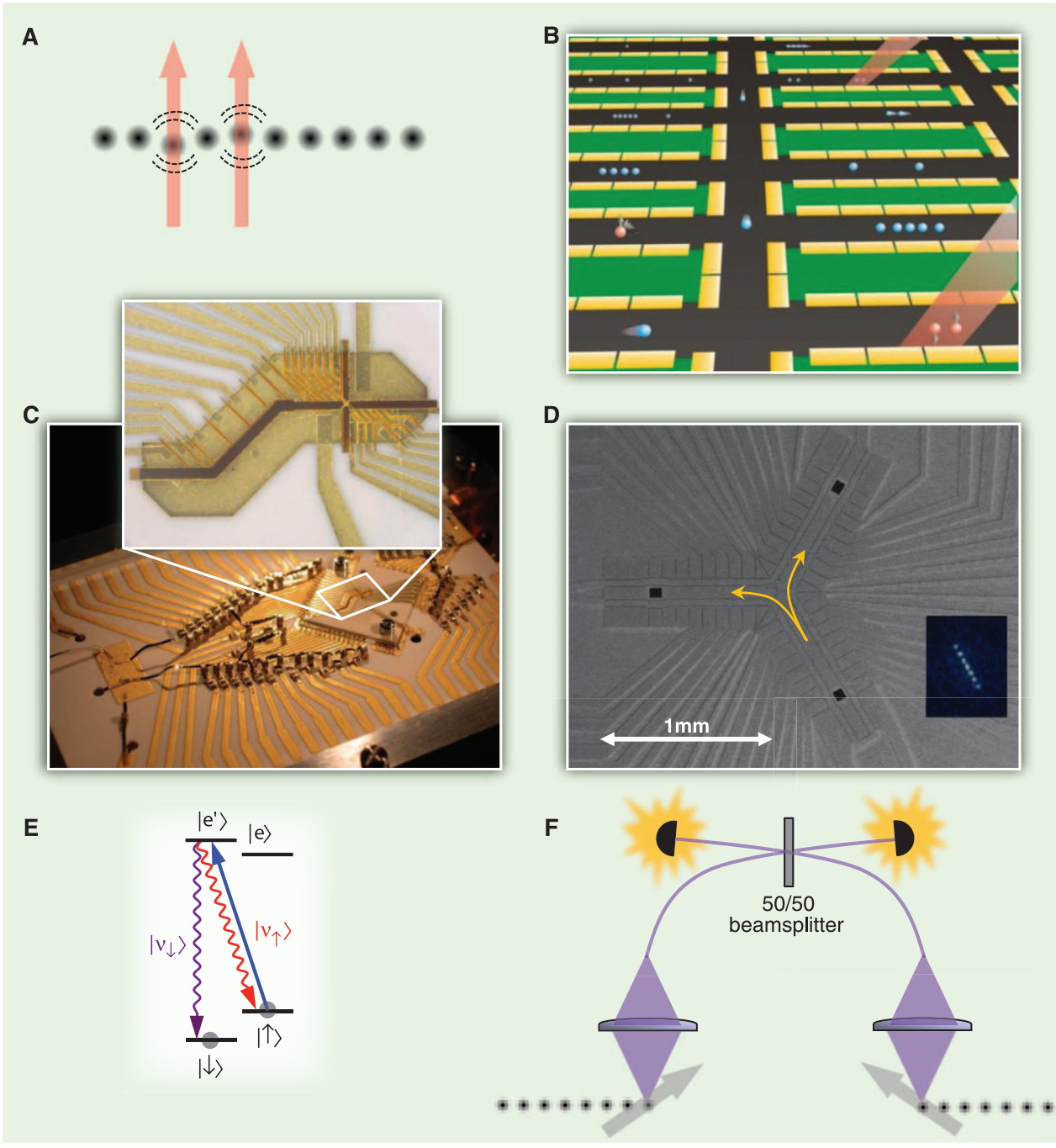

Fig. 2. (**A**) Optical dipole forces (red) displace two ions depending on their qubit states, and the resulting modulation of the Coulomb interaction allows the implementation of the controlled-NOT gate between these two ions. (**B**) Concept of a quantum CCD trap, in which ions can be shuttled between various zones. Ions can be entangled within a small crystal using laser forces as in (A) and then moved to different zones to propagate the entanglement to other ion crystals. Additional zones can be used for the loading of ions or qubit state detection. In principle, any pair of ions can be brought together through a web of ion trap channels, and a separate ion species can be used for sympathetic cooling to quench any residual motion from the shuttling procedure. [Image credit: National Institute of Standards and Technology] (**C**) Ion trap structure for the shuttling of ions through a junction. [Main image adapted with permission from (*18*); copyright 2011 by the American Physical Society] (**D**) Surface ion trap structure for shuttling ions through a three-channel junction. Inset shows an image of a trapped ion chain in lower right-hand sector. [Adapted with permission from (*19*); publisher: Institute of Physics] (**E**) Energy levels of trapped ion excited with a fast laser pulse (blue upward arrow) that produces single photon whose color, represented by the state $|\nu_{\uparrow}\rangle$ or $|\nu_{\downarrow}\rangle$, is entangled with the resultant qubit state $|\uparrow\rangle$ or $|\downarrow\rangle$, respectively. (**F**) Two "communication qubit" ions, immersed in separate crystals of other ions, each produce single photons when driven by laser pulses (blue). With some probability, the photons arrive at the 50/50 beamsplitter and then interfere. If the photons are indistinguishable (in polarization and color), then they always leave the beamsplitter along the same path. The simultaneous detection of photons at the two output detectors means that the photons were different colors, but because there is no knowledge of which color photon came from which ion emitter, this coincidence detection heralds the entanglement of the trapped ion qubits.

emitted by the *i*-th communication qubit. Here, we assume that the two photonic frequencies are distinguishable, or $|\nu_\uparrow - \nu_\downarrow| >> \gamma$, where γ is the radiative linewidth of the excited state. When two communication qubits *i* and *j* are excited in this way, and their photons are mode-matched on a 50/50 beamsplitter (Fig. 2F), the entanglement of the memories is heralded by the joint (coincidence) detection of photons at output detectors, creating the entangled state $|\downarrow\rangle_i|\uparrow\rangle_j - |\uparrow\rangle_j|\downarrow\rangle_i$ (*21*–*24*). This entanglement link succeeds with probability $p = (p_e F\eta_D)^2/2$, where F is the fraction of light collected from each emitter, and η_D is the single photon detector efficiency. Even though this is a probabilistic link, the detected photons indicate success, and the resulting entanglement between the ions can subsequently be used for deterministic quantum information processing. The mean connection rate is given by Rp, where R is the repetition rate of the initialization/excitation process, limited by the emission rate γ. For typical atomic transitions into free space with $\gamma \sim 10^8$/s, light collection fraction $F \sim 1$ to 10%, and detector efficiency $\eta_D \sim 20\%$, we find typical connection rates of 1 to 1000 Hz, with substantial gains possible with better photon collection strategies (*25*).

In practice, the communication qubit must be well isolated from the neighboring memory qubit ions so that scattered light from the excitation laser or the emitted photons themselves do not disturb the other memory qubits in each register. Although physical separation of the ions can provide the requisite isolation, a better solution is to use two different atomic species (*26*) to eliminate this crosstalk—for instance, $^{171}Yb^+$ for the memory qubit and $^{138}Ba^+$ for the communication qubit. Here, the communication qubits from separate registers become entangled via the photonic channel, and then the qubits within the communication ions are coherently mapped to neighboring memory qubits through Coulomb gates as described above.

New Technology for Scalability and Modularity

Scalable ion traps will require precision electrode structures, with as many discrete electrodes as trapped ion qubits, suggesting the use of micrometer-scale surface chip traps (*27*, *28*) that can be fabricated by using standard semiconductor processing techniques (*29*). Highly complex surface traps that can handle several tens of ions over tens of trapping zones have been fabricated and tested (Fig. 3, A and B) (*19*, *30*, *31*), with loading of up to ~10 ions with high-fidelity qubit preparation, detection, and single-qubit gate operations. Multi-qubit entangling operations in microscopic traps are more challenging because the ions experience higher levels of electric field noise from closer electrodes, causing motional decoherence during the gate operation. Although the source of this noise is still not well understood (*10*), it seems to scale roughly as $1/d^4$, where d is the characteristic distance from the ions to the nearest electrode (*32*). This motional heating can be quenched at cryogenic temperatures (*32*, *33*) or with adequate treatment of the trap surface (*34*), so this problem does not appear to be a fundamental limitation.

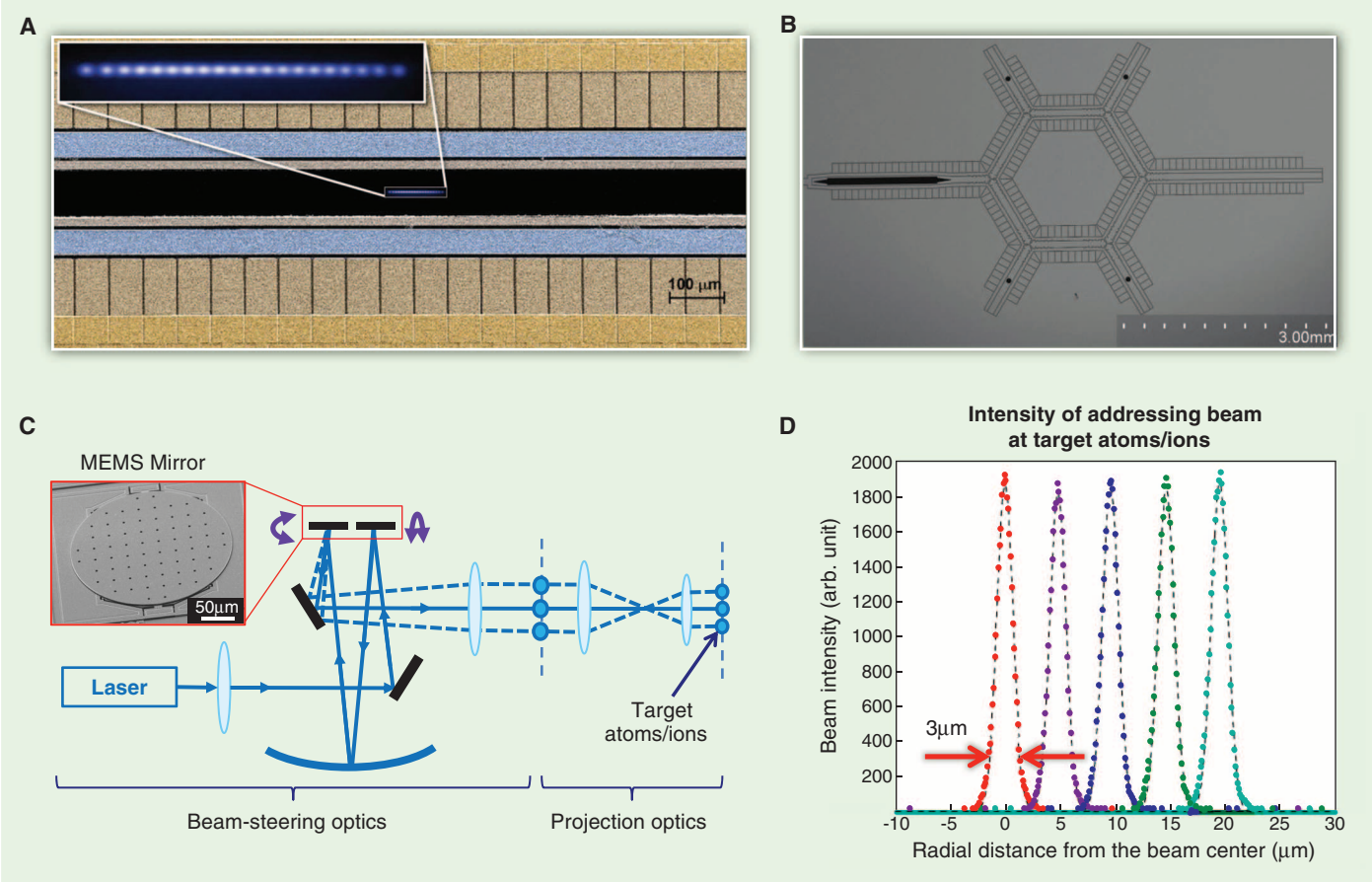

Fig. 3. (**A**) Scanning electron micrograph of a microfabricated linear trap with a long slot, with superimposed image of 20-ion chain in an anharmonic well (inset). The blue rails are RF electrodes and the rest are segments of static electrodes. [Courtesy GTRI] (**B**) Circulator trap with six junctions and two linear sections on either side for qubit manipulation. The other four short sections can be used as loading zones (of multiple ion species, if necessary), and the six junctions enable reordering of ions in the chain. [Courtesy Sandia National Laboratories] (**C**) Technology for individual optical addressing of ions in a linear chain. A control laser beam bounces off two MEMS mirrors tilting in orthogonal directions (inset) and can be steered over a two-dimensional space at the target atoms or ions. (**D**) The resulting profile of a ~3-μm diameter beam at 369.5 nm with a steering range of ~20 μm measured at the site of the ions.

Although the technology of trapping large numbers of ions has progressed, scaling the ability to individually address the qubits in the chain remains a challenge. Individual addressing of single atoms in an array via steering the control beam by using either electro-optic (EO) or acousto-optic deflectors has been demonstrated for small arrays (*35*, *36*). For larger atomic arrays, fast scanning mirrors provide an attractive solution (*37*, *38*). The advances in micro-electromechanical systems (MEMS) technology enable micromirror-based optical systems capable of independently steering multiple beams over the same atomic array (Fig. 3C).

A single ion chain (or several chains on a chip connected through the QCCD architecture) with an optical interface (Fig. 2F) can serve as a processor node (ELU) of a distributed quantum multicomputer, in which two-qubit gates between ions that belong to different ELUs are realized by using the photonic gate (*39*). When a large number ($\sim 10^3$) of such ELUs are connected through a reconfigurable photonic network supported by an optical crossconnect switch (*40*), a scalable quantum computer with up to $\sim 10^6$ qubits can be constructed (Fig. 4A). This architecture allows entanglement between any pair of ELUs in the processor with operations running in parallel, and distance-independent logic gate operations between any two qubits in the system. Such features are crucial for efficiently executing quantum algorithms that require nonlocal gates among the qubits and ensuring fault-tolerant quantum computation (*39*).

By conveying the photonic link over long distances, entanglement can be distributed between high-quality ion memory qubits separated by the distance traveled by the photons. Combined with the ability to perform local logic gates and high-fidelity measurements, each chip can thus serve as a quantum repeater node (Fig. 4B) that enables distribution of quantum entanglement over macroscopic distances by means of successive entanglement swapping (*41*). The photons adequate for carrying quantum information from ion qubits tend to have wavelengths in the ultraviolet or in the visible part of the spectrum, which is far from ideal for long-distance transmission. Quantum frequency converters can be used to translate the wavelength of the photon for better transmission (*42*). Shown in Fig. 4C is a schematic of a chain of quantum repeaters that enable entangled qubit pair distribution over macroscopic distances, which can be used for various quantum communication protocols, including quantum key distribution (QKD).

A major challenge in both modular quantum computer and quantum repeater applications is the slow rate of entanglement generation for the photonic gate, which is dominated by the low collection efficiency of the emitted photons. Continual efforts to improve collection of emitted photons into a single-mode fiber, involving the integration of ion traps with optical components such as mirrors (*43*), high numerical aperture lenses (*44*), and optical cavities (*45*), may boost the entanglement generation rate up by several orders of magnitude to above the decoherence rates of ion qubits.

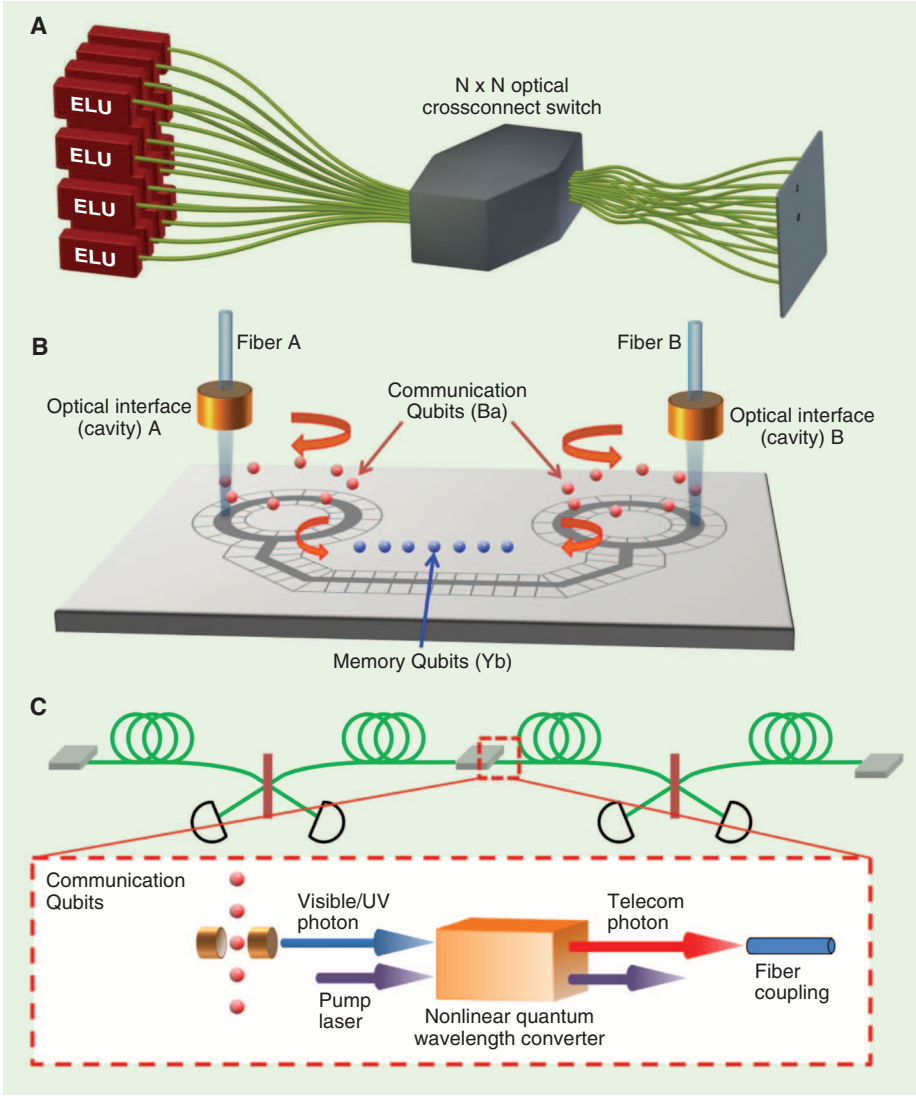

Fig. 4. Advanced quantum information systems with trapped ion technology. (**A**) Modular distributed quantum computer. Several ELUs are connected through a photonic network by using an optical crossconnect switch, inline fiber beamsplitters, and a photon-counting imager (*39*). [Adapted with permission from (*46*)] (**B**) Trapped ion quantum repeater node made up of communication qubit ions (such as Ba^+) and memory qubit ions (such as Yb^+), with two optical interfaces per node. Multiple communication qubits are used per optical interface to inject photons into the optical channel, while the results for successful entanglement generation at the detectors are reported back to this node. Only qubits corresponding to successful events will be transported to the memory qubit region for use in quantum repeater protocol. (**C**) A chain of quantum repeater nodes can distribute quantum entanglement over macroscopic distances. The photons generated by the ions must be converted to telecommunication wavelengths for long-distance transport, which can be achieved by nonlinear optical processes.

Outlook

The past decade has seen a number of small quantum information processors based on trapped ions, but in the coming years, we may see trapped ion devices used for applications that are difficult or impossible to perform using conventional technology. A quantum simulator that involves more than ~30 qubits may soon be able to predict behavior of interacting spin systems that is not tractable by a classical computer. Distribution of high-quality entangled qubit pairs over macroscopic distances by using trapped ion quantum repeaters may lead to new applications, such as long-distance QKD and multipartite entanglement distribution, as well as fundamental results, such as a loophole-free test of quantum nonlocality.

With the advent of microfabricated ion trap chips integrated with photonic components, modular ion trap quantum computer architectures

may lead to even larger quantum computers that can ultimately be put to use in materials design, communications, and high-performance computation. As quantum systems are made ever larger, they ultimately tend toward classical behavior because the quantum nature of the system quickly disappears even at the presence of tiny amounts of dissipation. Whether we find that the strange rules of quantum physics indeed persist to much larger systems, or perhaps a new order emerges, the trapped ion platform for quantum information processing is expected to provide the leading experimental playground in which to explore the evolution of complex quantum systems.

References and Notes

1. M. A. Nielsen, I. L. Chuang, *Quantum Computation and Quantum Information* (Cambridge Univ. Press, Cambridge, 2000).
2. C. R. Monroe, D. J. Wineland, *Sci. Am.* **299**, 64 (2008).
3. T. D. Ladd *et al.*, *Nature* **464**, 45 (2010).
4. D. Leibfried, R. Blatt, C. Monroe, D. Wineland, *Rev. Mod. Phys.* **75**, 281 (2003).
5. J. I. Cirac, P. Zoller, *Phys. Rev. Lett.* **74**, 4091 (1995).
6. A. Sørensen, K. Mølmer, *Phys. Rev. Lett.* **82**, 1971 (1999).
7. R. Blatt, D. Wineland, *Nature* **453**, 1008 (2008).
8. J. Benhelm, G. Kirchmair, C. F. Roos, R. Blatt, *Nat. Phys.* **4**, 463 (2008).
9. J. J. García-Ripoll, P. Zoller, J. I. Cirac, *Phys. Rev. Lett.* **91**, 157901 (2003).
10. Q. A. Turchette *et al.*, *Phys. Rev. A* **61**, 063418 (2000).
11. H. Häffner, C. Roos, R. Blatt, *Phys. Rep.* **469**, 155 (2008).
12. S.-L. Zhu, C. Monroe, L.-M. Duan, *Europhys. Lett.* **73**, 485 (2006).
13. J. Ignacio Cirac, P. Zoller, *Nat. Phys.* **8**, 264 (2012).
14. D. Kielpinski, C. Monroe, D. J. Wineland, *Nature* **417**, 709 (2002).
15. M. D. Barrett *et al.*, *Phys. Rev. A* **68**, 042302 (2003).
16. A. Walther *et al.*, *Phys. Rev. Lett.* **109**, 080501 (2012).
17. R. Bowler *et al.*, *Phys. Rev. Lett.* **109**, 080502 (2012).
18. R. B. Blakestad *et al.*, *Phys. Rev. A* **84**, 032314 (2011).
19. D. L. Moehring *et al.*, *New J. Phys.* **13**, 075018 (2011).
20. D. Gottesman, I. L. Chuang, *Nature* **402**, 390 (1999).
21. C. Simon, W. T. M. Irvine, *Phys. Rev. Lett.* **91**, 110405 (2003).
22. D. L. Moehring *et al.*, *Nature* **449**, 68 (2007).
23. C. Cabrillo, J. I. Cirac, P. Garcia-Fernandez, P. Zoller, *Phys. Rev. A* **59**, 1025 (1999).
24. L. Slodicka *et al.*, http://arxiv.org/abs/1207.5468 (2012).
25. T. Kim, P. Maunz, J. Kim, *Phys. Rev. A* **84**, 063423 (2011).
26. P. O. Schmidt *et al.*, *Science* **309**, 749 (2005).
27. J. Chiaverini *et al.*, *Quant. Inf. Comp.* **5**, 419 (2005).
28. S. Seidelin *et al.*, *Phys. Rev. Lett.* **96**, 253003 (2006).
29. J. Kim *et al.*, *Quant. Inf. Comput.* **5**, 515 (2005).
30. J. Amini *et al.*, *New J. Phys.* **12**, 033031 (2010).
31. J. T. Merrill *et al.*, *New J. Phys.* **13**, 103005 (2011).
32. L. Deslauriers *et al.*, *Phys. Rev. Lett.* **97**, 103007 (2006).
33. J. Labaziewicz *et al.*, *Phys. Rev. Lett.* **101**, 180602 (2008).
34. D. A. Hite *et al.*, *Phys. Rev. Lett.* **109**, 103001 (2012).
35. F. Schmidt-Kaler *et al.*, *Nature* **422**, 408 (2003).
36. D. D. Yavuz *et al.*, *Phys. Rev. Lett.* **96**, 063001 (2006).
37. C. Knoernschild *et al.*, *Appl. Phys. Lett.* **97**, 134101 (2010).
38. C. Weitenberg *et al.*, *Nature* **471**, 319 (2011).
39. C. Monroe *et al.*, http://arxiv.org/abs/1208.0391 (2012).
40. J. Kim *et al.*, *IEEE Photon. Technol. Lett.* **15**, 1537 (2003).
41. H.-J. Briegel, W.Dür, J. I. Cirac, P. Zoller, *Phys. Rev. Lett.* **81**, 5932 (1998).
42. K. De Greve *et al.*, *Nature* **491**, 421 (2012).
43. P. F. Herskind *et al.*, *Opt. Lett.* **36**, 3045 (2011).
44. A. Jechow, E. W. Streed, B. G. Norton, M. J. Petrasiunas, D. Kielpinski, *Opt. Lett.* **36**, 1371 (2011).
45. M. Steiner, H. M. Meyer, C. Deutsch, J. Reichel, M. Köhl, http://arxiv.org/abs/1211.0050 (2012).
46. L.-M. Duan, C. Monroe, *Rev. Mod. Phys.* **82**, 1209 (2010).

Acknowledgments: This work was supported by the U.S. Army Research Office (ARO) award W911NF0710576 with funds from the Defense Advanced Research Projects Agency (DARPA) Optical Lattice Emulator Program, ARO award W911NF0410234 with funds from the Intelligence Advanced Research Projects Activity Multi-Qubit Coherent Operations program, ARO Multidisciplinary University Initiative award W911NF0910406 on Hybrid Quantum Optical Circuits, Army Contracting Command award W31P4Q1210017 with funds from the DARPA Quiness Program, and the NSF Physics Frontier Center at JQI.

10.1126/science.1231298

REVIEW

Superconducting Circuits for Quantum Information: An Outlook

M. H. Devoret[1,2] and R. J. Schoelkopf[1]*

The performance of superconducting qubits has improved by several orders of magnitude in the past decade. These circuits benefit from the robustness of superconductivity and the Josephson effect, and at present they have not encountered any hard physical limits. However, building an error-corrected information processor with many such qubits will require solving specific architecture problems that constitute a new field of research. For the first time, physicists will have to master quantum error correction to design and operate complex active systems that are dissipative in nature, yet remain coherent indefinitely. We offer a view on some directions for the field and speculate on its future.

The concept of solving problems with the use of quantum algorithms, introduced in the early 1990s (*1*, *2*), was welcomed as a revolutionary change in the theory of computational complexity, but the feat of actually building a quantum computer was then thought to be impossible. The invention of quantum error correction (QEC) (*3*–*6*) introduced hope that a quantum computer might one day be built, most likely by future generations of physicists and engineers. However, less than 20 years later, we have witnessed so many advances that successful quantum computations, and other applications of quantum information processing (QIP) such as quantum simulation (*7*, *8*) and long-distance quantum communication (*9*), appear reachable within our lifetime, even if many discoveries and technological innovations are still to be made.

Below, we discuss the specific physical implementation of general-purpose QIP with superconducting qubits (*10*). A comprehensive review of the history and current status of the field is beyond the scope of this article. Several detailed reviews on the principles and operations of these circuits already exist (*11*–*14*). Here, we raise only a few important aspects needed for the discussion before proceeding to some speculations on future directions.

Toward a Quantum Computer

Developing a quantum computer involves several overlapping and interconnecting stages (Fig. 1). First, a quantum system has to be controlled sufficiently to hold one bit of quantum information long enough for it to be written, manipulated, and read. In the second stage, small quantum algorithms can be performed; these two stages require that the first five DiVincenzo criteria be satisfied (*15*). The following, more complex stages, however, introduce and require QEC (*3*–*6*). In the third stage, some errors can be corrected by quantum nondemolition readout of error syndromes such as parity. It also becomes possible to stabilize the qubit by feedback into any arbitrary state (*16*, *17*), including dynamical ones (*18*–*21*). This stage was reached first by trapped ions (*22*), by Rydberg atoms (*16*), and most recently by superconducting qubits (*23*–*25*). In the next (fourth) stage, the goal is to realize a quantum memory, where QEC realizes a coherence time that is longer than any of the individual components. This goal is as yet unfulfilled in any system. The final two stages in reaching the ultimate goal of fault-tolerant quantum information processing (*26*) require the ability to do all single-qubit operations on one logical qubit (which is an effective qubit protected by active error correction mechanisms), and the ability to perform gate operations between several logical qubits; in both stages the enhanced coherence lifetime of the qubits should be preserved.

Superconducting Circuits: Hamiltonians by Design

Unlike microscopic entities—electrons, atoms, ions, and photons—on which other qubits are based, superconducting quantum circuits are based on the electrical (LC) oscillator (Fig. 2A) and are macroscopic systems with a large number

[1]Departments of Applied Physics and Physics, Yale University, New Haven, CT 06520, USA. [2]College de France, Place Marcelin Berthelot, F-75005 Paris, France.

*To whom correspondence should be addressed. E-mail: robert.schoelkopf@yale.edu

of (usually aluminum) atoms assembled in the shape of metallic wires and plates. The operation of superconducting qubits is based on two robust phenomena: superconductivity, which is the frictionless flow of electrical fluid through the metal at low temperature (below the superconducting phase transition), and the Josephson effect, which endows the circuit with nonlinearity without introducing dissipation or dephasing.

The collective motion of the electron fluid around the circuit is described by the flux Φ threading the inductor, which plays the role of the center-of-mass position in a mass-spring mechanical oscillator (*27*). A Josephson tunnel junction transforms the circuit into a true artificial atom, for which the transition from the ground state to the excited state ($|g\rangle$-$|e\rangle$) can be selectively excited and used as a qubit, unlike in the pure LC harmonic oscillator (Fig. 2B). The Josephson junction can be placed in parallel with the inductor, or can even replace the inductor completely, as in the case of the so-called "charge" qubits. Potential energy functions of various shapes can be obtained by varying the relative strengths of three characteristic circuit energies associated with the inductance, capacitance, and tunnel element (Fig. 2, B and C). Originally, the three basic types were known as charge (*28*, *29*), flux (*30*–*33*), and phase (*34*, *35*). The performance of all types of qubits has markedly improved as the fabrication, measurement, and materials issues affecting coherence have been tested, understood, and improved. In addition, there has been a diversification of other design variations, such as the quantronium (*36*, *37*), transmon (*38*, *39*), fluxonium (*40*), and "hybrid" (*41*) qubits; all of these are constructed from the same elements but seek to improve performance by reducing their sensitivity to decoherence mechanisms encountered in earlier designs. The continuing evolution of designs is a sign of the robustness and future potential of the field.

When several of these qubits, which are nonlinear oscillators behaving as artificial atoms, are coupled to true oscillators (photons in a microwave cavity), one obtains, for low-lying excitations, an effective multiqubit, multicavity system Hamiltonian of the form

$$\frac{H_{\text{eff}}}{\hbar} = \sum_j \omega_j^q b_j^+ b_j + \frac{\alpha_j (b_j^+ b_j)^2}{2} + \sum_m \omega_m^r a_m^+ a_m + \sum_{j,m} \chi_{j,m} b_j^+ b_j a_m^+ a_m \quad (1)$$

describing anharmonic qubit mode amplitudes indexed by j coupled to harmonic cavity modes indexed by m (*42*). The symbols a, b, and ω refer to the mode amplitudes and frequency, respectively. When driven with appropriate microwave signals, this system can perform arbitrary quantum operations at speeds determined by the nonlinear interaction strengths α and χ, typically (*43*, *44*) resulting in single-qubit gate times within 5 to 50 ns ($\alpha/2\pi \approx 200$ MHz) and two-qubit entangling gate times within 50 to 500 ns ($\chi/2\pi \approx 20$ MHz). We have neglected here the weak induced anharmonicity of the cavity modes.

Proper design of the qubit circuit to minimize dissipation coming from the dielectrics surrounding the metal of the qubit, and to minimize radiation of energy into other electromagnetic modes or the circuit environment, led to qubit transition quality factors Q exceeding 1 million or coherence times on the order of 100 μs, which in turn make possible hundreds or even thousands of operations in one coherence lifetime (see Table 1). One example of this progression, for the case of the Cooper-pair box (*28*) and its descendants, is shown in Fig. 3A. Spectacular improvements have also been accomplished for transmission line resonators (*45*) and the other types of qubits, such the phase qubit (*35*) or the flux qubit (*46*). Rather stringent limits can now be placed on the intrinsic capacitive (*47*) or inductive (*43*) losses of the junction, and we construe this to mean that junction quality is not yet the limiting factor in the further development of superconducting qubits.

Nonetheless, it is not possible to reduce dissipation in a qubit independently of its readout and control systems (*39*). Here, we focus on the most useful and powerful type of readout, which is called a "quantum nondemolition" (QND) measurement. This type of measurement allows a continuous monitoring of the qubit state (*48*, *49*). After a strong QND measurement, the qubit is left in one of two computational states, $|g\rangle$ or $|e\rangle$, depending on the result of the measurement, which has a classical binary value indicating g or e. There are three figures of merit that characterize this type of readout. The first is QND-ness, the probability that the qubit remains in the same state after the measurement, given that the qubit is initially in a definite state $|g\rangle$ or $|e\rangle$. The second is the intrinsic fidelity, the difference between the probabilities—given that the qubit is initially in a definite state $|g\rangle$ or $|e\rangle$—that the readout gives the correct and wrong answers (with this definition, the fidelity is zero when the readout value is uncorrelated with the qubit state). The last and most subtle readout figure of merit is efficiency, which characterizes the ratio of the number of controlled and uncontrolled information channels in the readout. Maximizing this ratio is of utmost importance for performing remote entanglement by measurement (*50*).

Like qubit coherence, and benefiting from it, progress in QND performance has been spectacular (Fig. 3B). It is now possible to acquire more than $N = 2000$ bits of information from a qubit before it decays through dissipation (Fig. 3A), or, to phrase it more crudely, read a qubit once in a time that is a small fraction ($1/N$) of its lifetime. This is a crucial capability for undertaking QEC in the fourth stage of Fig. 1, because in order to fight errors, one has to monitor qubits at a pace faster than the rate at which they occur. Efficiencies in QND superconducting qubit readout are also progressing rapidly and will soon routinely exceed 0.5, as indicated by recent experiments (*25*, *51*).

Is It Just About Scaling Up?

Up to now, most of the experiments have been relatively small scale (only a handful of interacting qubits or degrees of freedom; see Table 1). Furthermore, almost all the experiments so far are

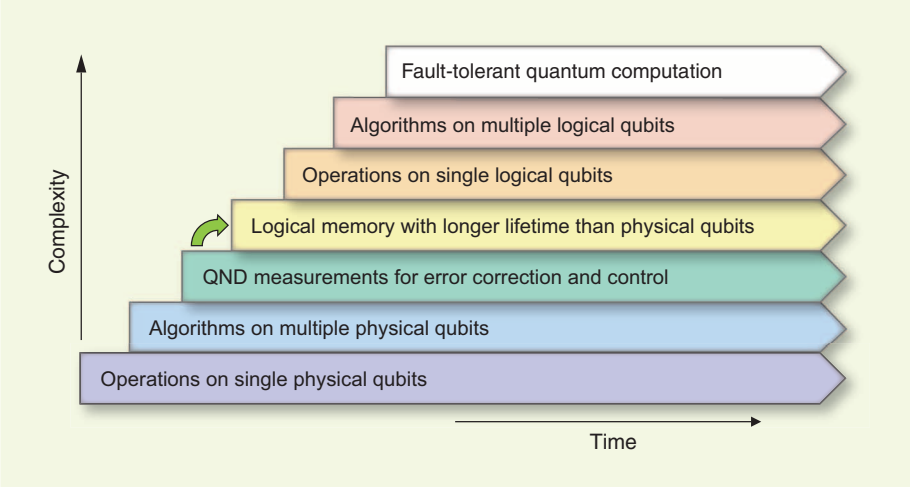

Fig. 1. Seven stages in the development of quantum information processing. Each advancement requires mastery of the preceding stages, but each also represents a continuing task that must be perfected in parallel with the others. Superconducting qubits are the only solid-state implementation at the third stage, and they now aim at reaching the fourth stage (green arrow). In the domain of atomic physics and quantum optics, the third stage had been previously attained by trapped ions and by Rydberg atoms. No implementation has yet reached the fourth stage, where a logical qubit can be stored, via error correction, for a time substantially longer than the decoherence time of its physical qubit components.

"passive"—they seek to maintain coherence only long enough to entangle quantum bits or demonstrate some rudimentary capability before, inevitably, decoherence sets in. The next stages of QIP require one to realize an actual increase in the coherence time via error correction, first only during an idle "memory" state, but later also in the midst of a functioning algorithm. This requires building new systems that are "active," using continuous measurements and real-time feedback to preserve the quantum information through the startling process of correcting qubit errors without actually learning what the computer is calculating. Given the fragility of quantum information, it is commonly believed that the continual task of error correction will occupy the vast majority of the effort and the resources in any large quantum computer.

Using the current approaches to error correction, the next stages of development unfortunately demand a substantial increase in complexity, requiring dozens or even thousands of physical qubits per bit of usable quantum information, and challenging our currently limited abilities to design, fabricate, and control a complex Hamiltonian (second part of Table 1). Furthermore, all of the DiVincenzo engineering margins on each piece of additional hardware still need to be maintained or improved while scaling up. So is advancing to the next stage just a straightforward engineering exercise of mass-producing large numbers of exactly the same kinds of circuits and qubits that have already been demonstrated? And will this mean the end of the scientific innovations that have so far driven progress forward?

We argue that the answers to both questions will probably be "No." The work by the community during the past decade and a half, leading up to the capabilities summarized in the first part of Table 1, may indeed constitute an existence proof that building a large-scale quantum computer is not physically impossible. However, identifying the best, most efficient, and most robust path forward in a technology's development is a task very different from merely satisfying oneself that it should be possible. So far, we have yet to see a dramatic "Moore's law" growth in the complexity of quantum hardware. What, then, are the main challenges to be overcome?

Simply fabricating a wafer with a large number of elements used today is probably not the hard part. After all, some of the biggest advantages of superconducting qubits are that they are merely circuit elements, which are fabricated in clean rooms, interact with each other via connections that are wired up by their designer, and are controlled and measured from the outside with electronic signals. The current fabrication requirements for superconducting qubits are not particularly daunting, especially in comparison to modern semiconductor integrated circuits (ICs). A typical qubit or resonant cavity is a few millimeters in overall size, with features that are mostly a few micrometers (even the smallest Josephson junction sizes are typically 0.2 μm on a side in a qubit). There is successful experience with fabricating and operating superconducting ICs with hundreds to thousands of elements on a chip, such as the transition-edge sensors with SQUID (superconducting quantum interference device) readout amplifiers, each containing several Josephson junctions (*52*), or microwave kinetic inductance detectors composed of arrays of high-Q ($>10^6$) linear resonators without Josephson junctions, which are being developed (*53*) and used to great benefit in the astrophysics community.

Nonetheless, designing, building, and operating a superconducting quantum computer presents substantial and distinct challenges relative to semiconductor ICs or the other existing versions of superconducting electronics. Conventional microprocessors use overdamped logic, which provides a sort of built-in error correction. They do not require high-Q resonances, and clocks or narrowband filters are in fact off-chip and provided by special elements such as quartz crystals. Therefore, small interactions between circuit elements may cause heating or offsets but do not lead to actual bit errors or circuit failures. In contrast, an integrated quantum computer will be essentially a very large collection of very high-Q, phase-stable oscillators, which need to interact only in the ways we program. It is no surprise that the leading quantum information technology has been and today remains the trapped ions, which are the best clocks ever built. In contrast with the ions, however, the artificially made qubits of a superconducting quantum computer will never be perfectly identical (see Table 1). Because operations on the qubits need to be controlled accurately to several significant digits, the properties of each part of the computer would first need to be characterized with some precision, have control signals tailored to match, and remain stable while the rest of the system is tuned up and then operated. The need for high absolute accuracy might therefore be circumvented if we can obtain a very high stability of qubit parameters (Table 1); recent results (*43*) are encouraging and exceed expectations, but more information is needed. The power of electronic control circuitry to tailor waveforms, such as composite pulse sequence techniques well known from nuclear magnetic resonance (*54*), can remove first-order sensitivity to variations in qubit parameters or in control signals, at the expense of some increase in gate time and a requirement for a concomitant increase in coherence time.

Even if the problem of stability is solved, unwanted interactions or cross-talk between the parts of these complex circuits will still cause problems. In the future, we must know and control the Hamiltonian to several digits, and for many qubits. This is beyond the current capability (~1 to 10%; see Table 1). Moreover, the number of measurements and the amount of data required

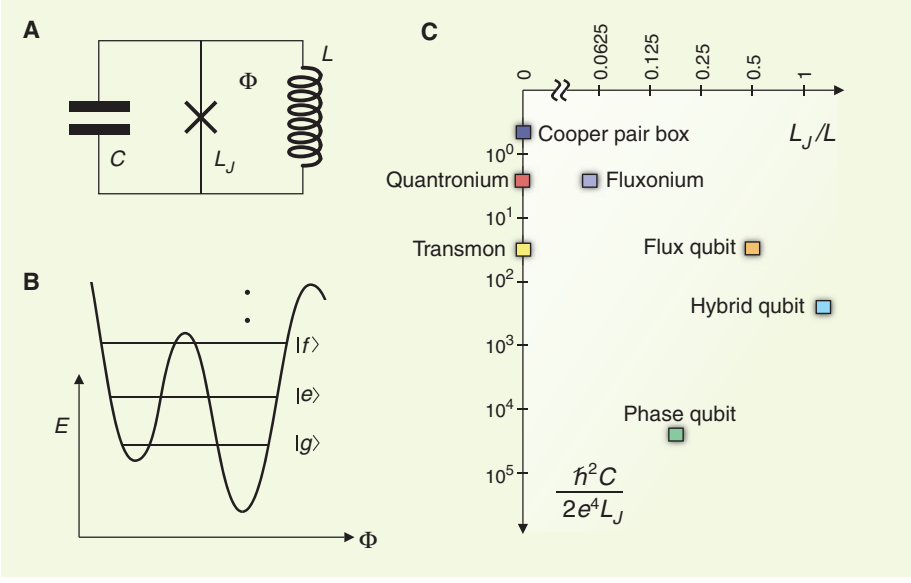

Fig. 2. (**A**) Superconducting qubits consist of simple circuits that can be described as the parallel combination of a Josephson tunnel element (cross) with inductance L_J, a capacitance C, and an inductance L. The flux Φ threads the loop formed by both inductances. (**B**) Their quantum energy levels can be sharp and long-lived if the circuit is sufficiently decoupled from its environment. The shape of the potential seen by the flux Φ and the resulting level structure can be varied by changing the values of the electrical elements. This example shows the fluxonium parameters, with an imposed external flux of ¼ flux quantum. Only two of three corrugations are shown fully. (**C**) A Mendeleev-like but continuous "table" of artificial atom types: Cooper pair box (*29*), flux qubit (*33*), phase qubit (*35*), quantronium (*37*), transmon (*39*), fluxonium (*40*), and hybrid qubit (*41*). The horizontal and vertical coordinates correspond to fabrication parameters that determine the inverse of the number of corrugations in the potential and the number of levels per well, respectively.

to characterize a system of entangled qubits appears to grow exponentially with their number, so the new techniques for "debugging" quantum circuits (*55*) will have to be further developed. In the stages ahead, one must design, build, and operate systems with more than a few dozen degrees of freedom, which, as a corollary to the power of quantum computation, are not even possible to simulate classically. This suggests that large quantum processors should perhaps consist of smaller modules whose operation and functionality can be separately tested and characterized.

A second challenge in Hamiltonian control (or circuit cross-talk) is posed by the need to combine long-lived qubits with the fast readout, qubit reset or state initialization, and high-speed controls necessary to perform error correction. This means that modes with much lower Q (~1000 for a 50-ns measurement channel) will need to be intimately mixed with the long-lived qubits with very high Q (~10^6 to 10^9), which requires exquisite isolation and shielding between the parts of our high-frequency integrated circuit. If interactions between a qubit and its surroundings cause even 0.1% of the energy of a qubit to leak into a low-Q mode, we completely spoil its lifetime. Although the required levels of isolation are probably feasible, these challenges have not yet been faced or solved by conventional superconducting or semiconducting circuit designers. In our view, the next stages of development will require appreciable advances, both practical and conceptual, in all aspects of Hamiltonian design and control.

What Will We Learn About Active Architectures During the Next Stage?

How long might it take to realize robust and practical error correction with superconducting circuits? This will depend on how rapidly the experimental techniques and capabilities (Fig. 3, A and B) continue to advance, but also on the architectural approach to QEC, which might considerably modify both the necessary circuit complexity and the performance limits (elements of Table 1) that are required. Several different approaches exist that are theoretically well developed (*1*, *2*) but remain relatively untested in the real world.

The canonical models for QEC are the stabilizer codes (*3*–*6*). Here, information is redundantly encoded in a register of entangled physical qubits (typically, at least seven) to create a single logical qubit. Assuming that errors occur singly, one detects them by measuring a set of certain collective properties (known as stabilizer operators) of the qubits, and then applies appropriate additional gates to undo the errors before the desired information is irreversibly corrupted. Thus, an experiment to perform gates between a pair of logically encoded qubits might take a few dozen qubits, with hundreds to thousands of individual operations. To reach a kind of "break-even" point and perform correctly, it is required that there should be less than one error on average during a single pass of the QEC. For a large calculation, the codes must then be concatenated, with each qubit again being replaced by a redundant register, in a treelike hierarchy. The so-called error-correction threshold, where the resources required for this process of expansion begin to converge, is usually estimated (*26*) to lie in the range of error rates of 10^{-3} to 10^{-4}, requiring values of 10^3 to 10^4 for the elements of Table 1. Although these performance levels and complexity requirements might no longer be inconceivable, they are nonetheless beyond the current state of the art, and rather daunting.

A newer approach (*56*–*58*) is the "surface code" model of quantum computing, where a large number of identical physical qubits are connected in a type of rectangular grid (or "fabric"). By having specific linkages between groups of four adjacent qubits, and fast QND measurements of their parity, the entire fabric is protected against errors. One appeal of this strategy is that it requires a minimum number of different types of elements, and once the development of the elementary cell is successful, the subsequent stages of development (the fourth, fifth, and sixth stages in Fig. 1) might simply be achieved by brute-force scaling. The second advantage is that the allowable error rates are appreciably higher, even on the order of current performance levels (a couple of percent). However, there are two drawbacks: (i) the resource requirements (between 100 and 10,000 physical qubits per logical qubit) are perhaps even higher than in the QEC codes (*58*), and (ii) the desired emergent properties of this fabric are obtained only after hundreds, if not thousands, of qubits have been assembled and tested.

A third strategy is based on modules of nested complexity. The basic element is a small register (*50*) consisting of a logical memory qubit, which stores quantum information while performing the usual kind of local error correction, and some additional communication qubits that can interact with the memory and with other modules. By entangling the communication qubits, one can distribute the entanglement and eventually perform a general computation between modules. Here, the operations between the communication bits can have relatively high error rates, or even be probabilistic and sometimes fail entirely, provided that the communication schemes have some modest redundancy and robustness. The adoption of techniques from cavity quantum electrodynamics (QED) (*59*) and the advantages for

Table 1. Superconducting qubits: Desired parameter margins for scalability and the corresponding demonstrated values. Desired capability margins are numbers of successful operations or realizations of a component before failure. For the stability of the Hamiltonian, capability is the number of Ramsey shots that meaningfully would provide one bit of information on a parameter (e.g., the qubit frequency) during the time when this parameter has not drifted. Estimated current capability is expressed as number of superconducting qubits, given best decoherence times and success probabilities. Demonstrated successful performance is given in terms of the main performance characteristic of successful operation or Hamiltonian control (various units). A reset qubit operation forces a qubit to take a particular state. A Rabi flop denotes a single-qubit π rotation. A swap to bus is an operation to make a two-qubit entanglement between distant qubits. In a readout qubit operation, the readout must be QND or must operate on an ancilla without demolishing any memory qubit of the computer. Stability refers to the time scale during which a Hamiltonian parameter drifts by an amount corresponding to one bit of information, or the time scale it would take to find all such parameters in a complex system to this precision. Accuracy can refer to the degree to which a certain Hamiltonian symmetry or property can be designed and known in advance, the ratio by which a certain coupling can be turned on and off during operation, or the ratio of desired to undesired couplings. Yield is the number of quantum objects with one degree of freedom that can be made without failing or being out of specification to the degree that the function of the whole is compromised. Complexity is the overall number of interacting, but separately controllable, entangled degrees of freedom in a device. Question marks indicate that more experiments are needed for a conclusive result. Values given in rightmost column are compiled from recently published data and improve on a yearly basis.

Requirement for scalability	Desired capability margins	Estimated current capability	Demonstrated successful performance
QI operation			
Reset qubit	10^2 to 10^4	50	Fidelity ≥ 0.995 (*17*)
Rabi flop	10^2 to 10^4	1000	Fidelity ≥ 0.99 (*69*, *70*)
Swap to bus	10^2 to 10^4	100	Fidelity ≥ 0.98 (*71*)
Readout qubit	10^2 to 10^4	1000	Fidelity ≥ 0.98 (*51*)
System Hamiltonian			
Stability	10^6 to 10^9	?	δff in 1 day < 2×10^{-7} (*43*)
Accuracy	10^2 to 10^4	10 to 100	1 to 10% (*43*)
Yield	>10^4	?	?
Complexity	10^4 to 10^7	10?	1 to 10 qubits (*61*)

routing microwave photons with transmission lines [now known as circuit QED (*12*, *44*, *60*)] might make on-chip versions of these schemes with superconducting circuits an attractive alternative. Although this strategy can be viewed as less direct and requires a variety of differing parts, its advantage is that stringent quality tests are easier to perform at the level of each module, and hidden design flaws might be recognized at earlier stages. Finally, once modules with sufficient performance are in hand, they can then be programmed to realize any of the other schemes in an additional "software layer" of error correction.

Finally, the best strategy might include ideas that are radically different from those considered standard fare in quantum information science. Much may be gained by looking for shortcuts that are hardware-specific and optimized for the particular strengths and weaknesses of a particular technology. For instance, all of the schemes described above are based on a "qubit register model," where one builds the larger Hilbert space and the required redundancy from a collection of many individual two-level systems. But for superconducting circuits, the "natural units" are oscillators with varying degrees of nonlinearity, rather than true two-level systems. The use of noncomputational states beyond the first two levels is of course known in atomic physics, and has already been used as a shortcut to two- and three-qubit gates in superconducting circuits (*23*, *61*). Under the right conditions, the use of nonlinear oscillators with many accessible energy levels could replace the function of several qubits without introducing new error mechanisms. As a concrete example of the power of this approach, a recent proposal (*62*) for using a cavity as a protected memory requires only one ancilla and one readout channel—a real decrease in complexity.

How architectural choices like these affect our ability to perform error-corrected information processing will be a key scientific question occupying this field in the near future, and will probably take several years to resolve. The knowledge garnered in this process has the potential to substantially change the resources required for building quantum computers, quantum simulators, or quantum communication systems that are actually useful.

The Path Forward

The field of QIP with superconducting circuits has made dramatic progress, and has already demonstrated most of the basic functionality with reasonable (or even surprising) levels of performance. Remarkably, we have not yet encountered any fundamental physical principles that would prohibit the building of quite large quantum processors. The demonstrated capabilities of superconducting circuits, as in trapped ions and cold atoms, mean that QIP is beginning what may be one of its most interesting phases of development. Here, one enters a true terra incognita for complex quantum systems, as QEC becomes more than a theoretical discipline. As in the past, this era will include new scientific innovations and basic questions to be answered. Even if this stage is successful, there will remain many further stages of development and technical challenges to be mastered before useful quantum information processing could become a reality. However, we think it is unlikely to become a purely technological enterprise, like sending a man to the Moon, in the foreseeable future. After all, even the Moore's law progression of CMOS integrated circuits over the past four decades has not brought the end of such fields as semiconductor physics or nanoscience, but rather enabled, accelerated, and steered them in unanticipated directions. We feel that future progress in quantum computation will always

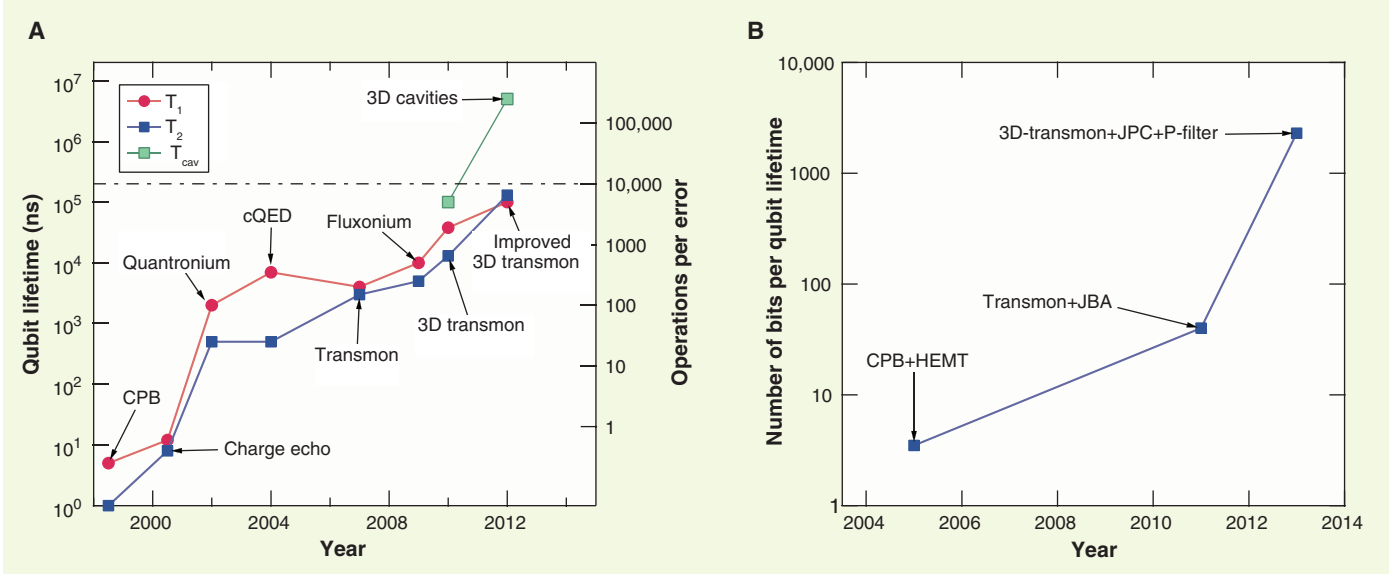

Fig. 3. Examples of the "Moore's law" type of exponential scaling in performance of superconducting qubits during recent years. All types have progressed, but we focus here only on those in the leftmost part of Fig. 2C. (**A**) Improvement of coherence times for the "typical best" results associated with the first versions of major design changes. The blue, red, and green symbols refer to qubit relaxation, qubit decoherence, and cavity lifetimes, respectively. Innovations were introduced to avoid the dominant decoherence channel found in earlier generations. So far an ultimate limit on coherence seems not to have been encountered. Devices other than those in Fig. 2C: charge echo (*63*), circuit QED (*44*), 3D transmon (*43*), and improved 3D transmon (*64*, *65*). For comparison, superconducting cavity lifetimes are given for a 3D transmon and separate 3D cavities (*66*). Even longer times in excess of 0.1 s have been achieved in similar 3D cavities for Rydberg atom experiments [e.g., (*67*)]. (**B**) Evolution of superconducting qubit QND readout. We plot versus time the main figure of merit, the number of bits that can be extracted from the qubit during its T1 lifetime (this number combines signal-to-noise ratio and speed). This quantity can also be understood as the number of measurements, each with one bit of precision, that would be possible before an error occurs. Data points correspond to the following innovations in design: a Cooper-pair box read by off-resonance coupling to a cavity whose frequency is monitored by a microwave pulse analyzed using a semiconductor high–electron mobility transistor amplifier (CPB+HEMT) [also called dispersive circuit QED (*68*)], an improved amplification chain reading a transmon using a superconductor preamplifier derived from the Josephson bifurcation amplifier (transmon+JBA) (*49*), and further improvement with another superconductor preamplifier derived from the Josephson parametric converter (*51*) combined with filter in 3D transmon cavity eliminating Purcell effect (3D-transmon+JPC+P-filter). Better amplifier efficiency, optimal signal processing, and longer qubit lifetimes are expected to maintain the rapid upward trend.

require the robust, continual development of both scientific understanding and engineering skill within this new and fascinating arena.

References and Notes

1. M. A. Nielsen, I. L. Chuang, *Quantum Computation and Quantum Information* (Cambridge Univ. Press, Cambridge, 2000).
2. N. D. Mermin, *Quantum Computer Science* (Cambridge Univ. Press, Cambridge, 2007).
3. P. W. Shor, *Phys. Rev. A* **52**, R2493 (1995).
4. A. Steane, *Proc. R. Soc. London Ser. A* **452**, 2551 (1996).
5. E. Knill, R. Laflamme, *Phys. Rev. A* **55**, 900 (1997).
6. D. Gottesman, thesis, California Institute of Technology (1997).
7. S. Lloyd, *Science* **273**, 1073 (1996).
8. See, for example, J. I. Cirac, P. Zoller, Goals and opportunities in quantum simulations. *Nat. Phys.* **8**, 264 (2012) and other articles in this special issue.
9. H. J. Kimble, *Nature* **453**, 1023 (2008).
10. Direct quantum spin simulations, such as aimed at by the machine constructed by D-Wave Systems Inc., are outside the scope of this article.
11. M. H. Devoret, J. M. Martinis, *Quant. Inf. Proc.* **3**, 381 (2004).
12. R. J. Schoelkopf, S. M. Girvin, *Nature* **451**, 664 (2008).
13. J. Clarke, F. K. Wilhelm, *Nature* **453**, 1031 (2008).
14. J. Q. You, F. Nori, *Phys. Today* **58**, 42 (2005).
15. D. P. DiVincenzo, *Fortschr. Phys.* **48**, 771 (2000).
16. C. Sayrin *et al.*, *Nature* **477**, 73 (2011).
17. K. Geerlings *et al.*, http://arxiv.org/abs/1211.0491 (2012).
18. R. Vijay *et al.*, *Nature* **490**, 77 (2012).
19. K. W. Murch *et al.*, *Phys. Rev. Lett.* **109**, 183602 (2012).
20. S. Diehl *et al.*, *Nat. Phys.* **4**, 878 (2008).
21. J. T. Barreiro *et al.*, *Nature* **470**, 486 (2011).
22. P. Schindler *et al.*, *Science* **332**, 1059 (2011).
23. M. D. Reed *et al.*, *Nature* **482**, 382 (2012).
24. D. Ristè, C. C. Bultink, K. W. Lehnert, L. DiCarlo, *Phys. Rev. Lett.* **109**, 240502 (2013).
25. P. Campagne-Ibarq *et al.*, http://arxiv.org/abs/1301.6095 (2013).
26. J. Preskill, http://arxiv.org/abs/quant-ph/9712048 (1997).
27. M. H. Devoret, in *Quantum Fluctuations*, S. Reynaud, E. Giacobino, J. Zinn-Justin, Eds. (Elsevier Science, Amsterdam, 1997).
28. V. Bouchiat, D. Vion, P. Joyez, D. Esteve, M. H. Devoret, *Phys. Scr.* **1998**, 165 (1998).
29. Y. Nakamura, Yu. A. Pashkin, J. S. Tsai, *Nature* **398**, 786 (1999).
30. J. E. Mooij *et al.*, *Science* **285**, 1036 (1999).
31. C. H. van der Wal *et al.*, *Science* **290**, 773 (2000).
32. J. R. Friedman, V. Patel, W. Chen, S. K. Tolpygo, J. E. Lukens, *Nature* **406**, 43 (2000).
33. I. Chiorescu, Y. Nakamura, C. J. Harmans, J. E. Mooij, *Science* **299**, 1869 (2003).
34. J. M. Martinis, S. Nam, J. Aumentado, C. Urbina, *Phys. Rev. Lett.* **89**, 117901 (2002).
35. J. Martinis, *Quant. Inf. Proc.* **8**, 81 (2009).
36. A. Cottet *et al.*, *Physica C* **367**, 197 (2002).
37. D. Vion *et al.*, *Science* **296**, 886 (2002).
38. J. Koch *et al.*, *Phys. Rev. A* **76**, 042319 (2007).
39. A. A. Houck *et al.*, *Phys. Rev. Lett.* **101**, 080502 (2008).
40. V. E. Manucharyan, J. Koch, L. I. Glazman, M. H. Devoret, *Science* **326**, 113 (2009).
41. M. Steffen *et al.*, *Phys. Rev. Lett.* **105**, 100502 (2010).
42. S. E. Nigg *et al.*, *Phys. Rev. Lett.* **108**, 240502 (2012).
43. H. Paik *et al.*, *Phys. Rev. Lett.* **107**, 240501 (2011).
44. A. Wallraff *et al.*, *Nature* **431**, 162 (2004).
45. A. Megrant *et al.*, *Appl. Phys. Lett.* **100**, 113510 (2012).
46. J. Bylander *et al.*, *Nat. Phys.* **7**, 565 (2011).
47. Z. Kim *et al.*, *Phys. Rev. Lett.* **106**, 120501 (2011).
48. A. Palacios-Laloy *et al.*, *Nat. Phys.* **6**, 442 (2010).
49. R. Vijay, D. H. Slichter, I. Siddiqi, *Phys. Rev. Lett.* **106**, 110502 (2011).
50. L. M. Duan, B. B. Blinov, D. L. Moehring, C. Monroe, *Quantum Inf. Comput.* **4**, 165 (2004).
51. M. Hatridge *et al.*, *Science* **339**, 178 (2013).
52. D. Bintley *et al.*, *Proc. SPIE* **8452**, 845208 (2012).
53. J. Zmuidzinas, *Annu. Rev. Condens. Matter Phys.* **3**, 169 (2012).
54. J. Jones, NMR Quantum Computation (nmr.physics.ox.ac.uk/pdfs/lhnmrqc.pdf).
55. M. P. da Silva, O. Landon-Cardinal, D. Poulin, *Phys. Rev. Lett.* **107**, 210404 (2011).
56. S. Bravyi, A. Yu. Kitaev, *Quantum Computers Comput.* **2**, 43 (2001).
57. M. H. Freedman, D. A. Meyer, *Found. Comput. Math.* **1**, 325 (2001).
58. A. G. Fowler, M. Mariantoni, J. M. Martinis, A. N. Cleland, *Phys. Rev. A* **86**, 032324 (2012).
59. S. Haroche, J. M. Raimond, *Exploring the Quantum: Atoms, Cavities, and Photons* (Oxford Univ. Press, Oxford, 2006).
60. C. Eichler *et al.*, *Phys. Rev. Lett.* **106**, 220503 (2011).
61. M. Mariantoni *et al.*, *Nat. Phys.* **7**, 287 (2011).
62. Z. Leghtas *et al.*, http://arxiv.org/abs/1207.0679.
63. Y. Nakamura, Y. A. Pashkin, T. Yamamoto, J. S. Tsai, *Phys. Rev. Lett.* **88**, 047901 (2002).
64. A. Sears *et al.*, *Phys. Rev. B* **86**, 180504 (2012).
65. C. Rigetti *et al.*, *Phys. Rev. B* **86**, 100506 (2012).
66. M. Reagor *et al.*, http://arxiv.org/abs/1302.4408 (2013).
67. S. Kuhr *et al.*, *Appl. Phys. Lett.* **90**, 164101 (2007).
68. A. Wallraff *et al.*, *Phys. Rev. Lett.* **95**, 060501 (2005).
69. E. Magesan *et al.*, *Phys. Rev. Lett.* **109**, 080505 (2012).
70. E. Lucero *et al.*, *Phys. Rev. Lett.* **100**, 247001 (2008).
71. J. M. Chow *et al.*, *Phys. Rev. Lett.* **109**, 060501 (2012).

Acknowledgments: We thank L. Frunzio, S. Girvin, L. Glazman, and L. Jiang for their contributions. Supported by the U.S. Army Research Office, U.S. National Security Agency Laboratory for Physical Science, U.S. Intelligence Advanced Research Projects Activity, NSF, and Yale University.

10.1126/science.1231930

REVIEW

Quantum Spintronics: Engineering and Manipulating Atom-Like Spins in Semiconductors

David D. Awschalom,[1]* Lee C. Bassett,[1] Andrew S. Dzurak,[2] Evelyn L. Hu,[3] Jason R. Petta[4]

The past decade has seen remarkable progress in isolating and controlling quantum coherence using charges and spins in semiconductors. Quantum control has been established at room temperature, and electron spin coherence times now exceed several seconds, a nine–order-of-magnitude increase in coherence compared with the first semiconductor qubits. These coherence times rival those traditionally found only in atomic systems, ushering in a new era of ultracoherent spintronics. We review recent advances in quantum measurements, coherent control, and the generation of entangled states and describe some of the challenges that remain for processing quantum information with spins in semiconductors.

In a marriage of quantum physics, information theory, and nanoscale engineering, quantum information science endeavors to build machines that can use the power of quantum mechanics for practical purposes. Such machines have great potential, including cryptography guaranteed by the laws of physics, quantum-enhanced sensing and imaging technology, and quantum computers able to crack problems inaccessible to even the most powerful classical computers of the foreseeable future.

The complexity of building quantum machines is a fantastic challenge, and recent years have seen a vast array of proposals for quantum information processing in diverse systems. Although specific requirements vary considerably, there are a few generalized prerequisites for quantum computers (*1*). The target quantum system must be controllable, in the sense that it can be initialized, manipulated, and read out to achieve a computation; it must be correctable, such that unavoidable errors can be detected and compensated; and it must be scalable, such that a linear increase in the effective size of the system—corresponding to an exponential increase in computing power—does not require an exponential increase of resources. The first two requirements require some degree of isolation of the quantum system from its environment, to keep quantum information from "leaking away" (decohering) at a rate faster than the computation is achieved. Because no system is entirely free of decoherence, the goal of most approaches is to balance the need for isolation with the ability to accurately and quickly control the system, ideally in architectures with potential for scaling to larger systems once the fundamentals are established.

[1]Center for Spintronics and Quantum Computation, University of California, Santa Barbara, Santa Barbara, CA 93106, USA. [2]Centre for Quantum Computation and Communication Technology, School of Electrical Engineering and Telecommunications, The University of New South Wales, Sydney 2052, Australia. [3]School of Engineering and Applied Sciences, Harvard University, Cambridge, MA 02138, USA. [4]Department of Physics, Princeton University, Princeton, NJ 08544, USA.

*To whom correspondence should be addressed. E-mail: awsch@physics.ucsb.edu

Nature's own atoms and ions, isolated in vacuum, served as the first quantum information test beds, with many groundbreaking experiments in atomic and optical physics demonstrating exquisite control of individual quantum systems. Inspired by this success, solid-state physicists have recently developed a wide array of "designer atoms" based on semiconductor nanostructures whose quantum states can also be coherently controlled (*2*). The spins of individual electrons and nuclei, in particular, offer a promising combination of environmental isolation and controllability, with wide flexibility in terms of materials and design. Furthermore, solid-state technologies offer the promise of large-scale integration using fabrication processes developed by the semiconductor industry (*3*). Approaches are markedly varied, employing different materials, temperatures, device structures, and both electrical and optical measurements. We focus on several key advances of the past few years in controlling quantum coherence and entanglement in several semiconductor architectures, and outline the major challenges and goals ahead.

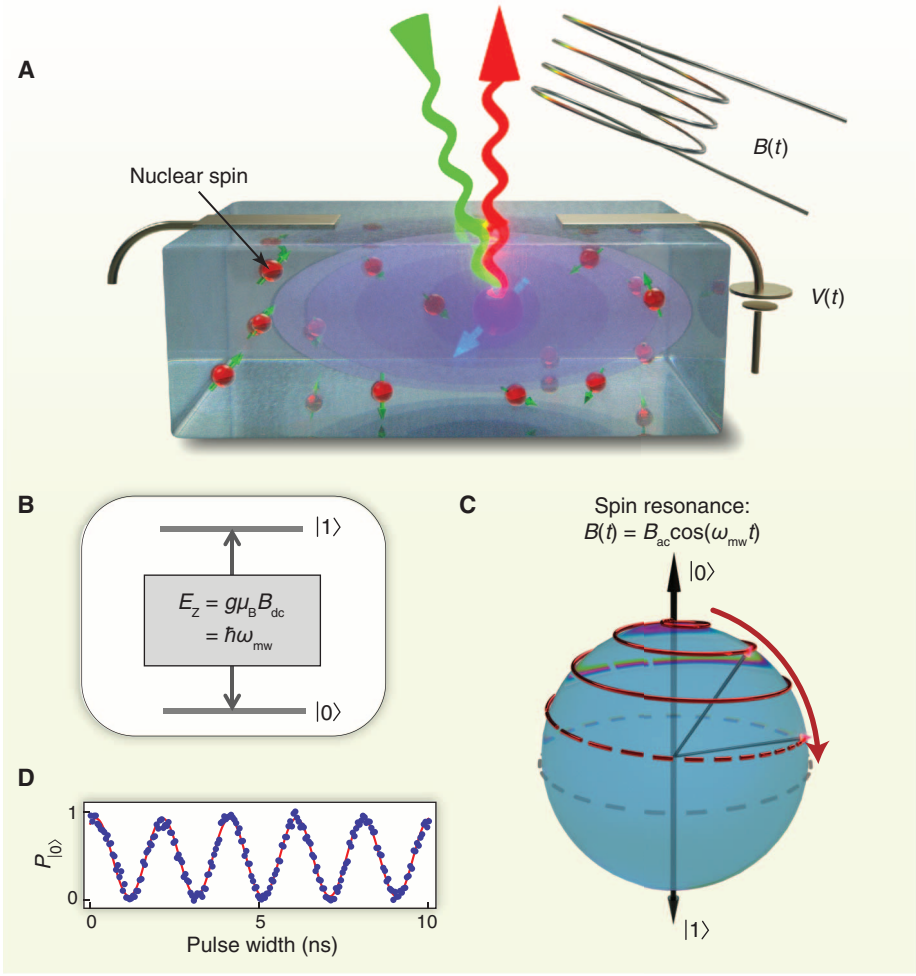

Fig. 1. (**A**) Single electron spins (blue arrow) can be confined in solid-state systems and manipulated with various "control knobs," including gate voltages [$V(t)$], microwave magnetic fields [$B(t)$], and light (green and red wiggly arrows). Quantum coherence is lost (fading purple cloud) through interactions with the local environment of, for example, nuclear spins (green arrows), phonons, or leaky mirrors in a cavity. Recent advances in materials science have made it possible to achieve electron spin coherence times up to several seconds (*15*), rivaling those traditionally found only in atomic systems. (**B**) A single electron spin placed in a dc magnetic field, B_{dc}, forms a quantum bit with states $|0\rangle$ and $|1\rangle$ corresponding to parallel and antiparallel spin alignment to the field, split by the Zeeman energy E_Z. (**C**) The application of an oscillating magnetic field $B(t)$ perpendicular to B_{dc} and resonant with the Zeeman energy causes the qubit to oscillate between states $|0\rangle$ and $|1\rangle$ at the Rabi frequency (changing the qubit amplitude, θ), while the phase ϕ accumulates due to precession in B_{dc}. (**D**) Rabi nutations of a single electronic spin in diamond, measured optically, showing the probability to measure the state $|0\rangle$ as a function of the width of an ac magnetic field pulse. Conventional electron spin resonance has focused on the dynamics of large ensembles of $\gtrsim 10^{15}$ spins; it has recently become possible to coherently control single-spin dynamics. [Originally published in (*60*) and adapted with permission]

Spin Qubits for Computation

The spin carried by a single electron is a prototypical quantum bit, or qubit (Fig. 1A). In an external magnetic field, B_{dc}, the spin's energy levels are quantized into states where the magnetic moment points either parallel or antiparallel to the magnetic field. These two states are separated by the Zeeman energy, $E_Z = g\mu_B B_{dc}$, where g is the Landé g factor and μ_B is the Bohr magneton (Fig. 1B). By identifying one spin orientation as "0" and the other as "1," spins can serve as the logical elements for Boolean computation. Even as classical bits, spins offer advantages over today's charge-based microprocessors and form the basis for emerging technologies termed spintronics. The more ambitious goal of building a spin-based quantum computer requires not only manipulation of the spin eigenstates $|0\rangle$ and $|1\rangle$ but also coherent superpositions of the form $|\psi\rangle = \cos(\theta/2)|0\rangle + e^{i\phi}\sin(\theta/2)|1\rangle$, where both the amplitude, θ, and the phase, ϕ, must be controlled with high precision. Most challengingly, quantum computing requires the creation and coherent control of nonclassical correlations—i.e., entanglement—between distinct qubits in the device and preservation of these fragile many-body states on time scales long enough to perform calculations. At the few-qubit level, both of these goals have been met in recent years.

As qubits, spins in semiconductors have distinct technical advantages. Host-dependent band structure and spin-orbit interactions imprint critical characteristics on spins in different materials, providing widely tunable qubit properties. Particularly in materials where spin-orbit coupling is weak, spins are relatively insensitive to many sources of decoherence in solid-state systems, including electrical noise and thermal vibrations of the semiconductor lattice. Furthermore, experimental methods for coherent control of single-spin qubit states are now established (Fig. 1C), building on decades of research in magnetic resonance. Figure 2 shows examples of four types of spin qubits featured in current research. Despite vastly different methods for production and individual advantages and challenges of the different systems, coherent quantum control of individual qubits has been demonstrated in all cases, and in several systems entangled multiqubit devices have been realized in recent years.

Following a proposal based on spins in quantum dots (*4*), the first semiconductor qubits were based on group III/V materials (*5*), taking advantage of the well-developed growth of ultrapure GaAs/AlGaAs heterostructures. Heterostructures provide the means to confine electrons and/or holes into reduced dimensions, to the ultimate limit of a zero-dimensional "box"—a quantum dot (QD)—containing a single spin. QDs can be formed either through top-down approaches

in which nanofabricated surface electrodes deplete charges from a buried two-dimensional electron gas (Fig. 2A) or through bottom-up growth techniques in which small islands of a III/V alloy, typically InAs, self-assemble on a GaAs surface (Fig. 2B).

The small magnetic moment of the electron renders it highly insensitive to the local environment, leading to long spin coherence times. At the same time, however, rapid spin control using conventional electron spin resonance requires large ac magnetic field amplitudes that are difficult to produce in cryogenic environments. Qubit selectivity is also exacerbated in nanoscale devices (Fig. 2A), where each spin needs to be individually controlled without disturbing its nearest neighbors only ≈50 nm away. Two approaches have been developed to circumvent these challenges. The first is to use quantum interference of two-electron spin states for rapid quantum control. By rapidly tuning through an avoided crossing in the energy-level diagram, two electrons in a correlated (e.g., singlet) state can be "split" and then recombined after a free evolution time, enabling nanosecond spin rotations without the application of an electron spin resonance field (*6*). Another approach to single-spin control harnesses the strong spin-orbit interactions intrinsic to materials such as InAs and InSb. With such "spin-orbit qubits," it is possible to perform spin rotations using electric rather than magnetic fields, which are easier to generate and localize in a device (*7*).

Self-assembled QDs in III/V materials confine both electrons and holes and can therefore support optical transitions between a ground-state spin qubit configuration (e.g., a single electron or hole) and optically excited "excitons" with additional bound electron-hole pairs. Strong spin-orbit interactions give rise to optical transitions with strict spin- and polarization-dependent selection rules, and relatively large optical dipole moments (compared with atoms) make these transitions highly efficient. These key features enable coherent optical control of the QD spin state using ultrafast (picosecond-scale) pulses of light (*8*, *9*) and the generation of entanglement between the qubit spin state and a single photon emitted by the QD (*10*, *11*). Such light-matter coupling is the key to building distributed networks of qubit nodes with coherent information transfer mediated by photons.

Only a few years ago, the intrinsic "spin bath" of host nuclear spins in III/V materials was the primary impediment to achieving long spin coherence times in these systems. This problem has been practically solved through the use of dynamical decoupling protocols that can extend the useful coherence time by orders of magnitude (*12*–*14*). Still, it helps to remove as many potential noise sources as possible. Group IV semiconductors can be isotopically purified to provide a nearly spin-free environment consisting only of spin-zero nuclei such as ^{12}C and ^{28}Si, and weaker spin-orbit coupling than in III/V materials reduce susceptibility to electrical and thermal noise. With recent reports of electron-spin coherence times measured in seconds (*15*) and nuclear spin coherence times of minutes (*16*) for neutral donor atoms in ^{28}Si, for example, these materials are poised to have a major role in coming years.

Silicon, the dominant material used for conventional microprocessor chips, was identified early on as a prime candidate for quantum information processing through several proposals to use the electron and/or nuclear spins of individual donor atoms, particularly phosphorus, as spin qubits (*17*, *18*). The first such single-atom qubit in silicon (Fig. 2C) used the spin of a phosphorus donor electron implanted into a silicon chip as the qubit (*19*). An adjacent metal-oxide-semiconductor–based single-electron transistor implements a spin-to-charge conversion protocol for initialization and readout (*20*) similar to that developed for III/V quantum dots (*21*), and coherent control is achieved through electron spin resonance using an integrated microwave transmission line. Fabricated using a silicon substrate with the natural 4.7% isotopic fraction of ^{29}Si, the spin coherence time of the device in (*19*) was limited by the nuclear spin bath to $T_2 \approx 200$ μs, but it is anticipated that similar devices constructed from isotopically enriched ^{28}Si substrates will open a path to the exceptional coherence times (≈1 s) that have been measured for bulk ^{28}Si:P ensembles (*15*). The device depicted in Fig. 2C has also been used to demonstrate a nuclear spin qubit (*22*) based on the ^{31}P dopant nucleus. These nuclear spins could serve as long-lived quantum memories (*18*) in future quantum processors.

In some ways, dopant-based qubits in silicon represent a powerful combination of both top-down and bottom-up fabrication approaches, because a natural and highly reproducible qubit (a single atom) is controllably placed within a nanofabricated electronic device. At the same

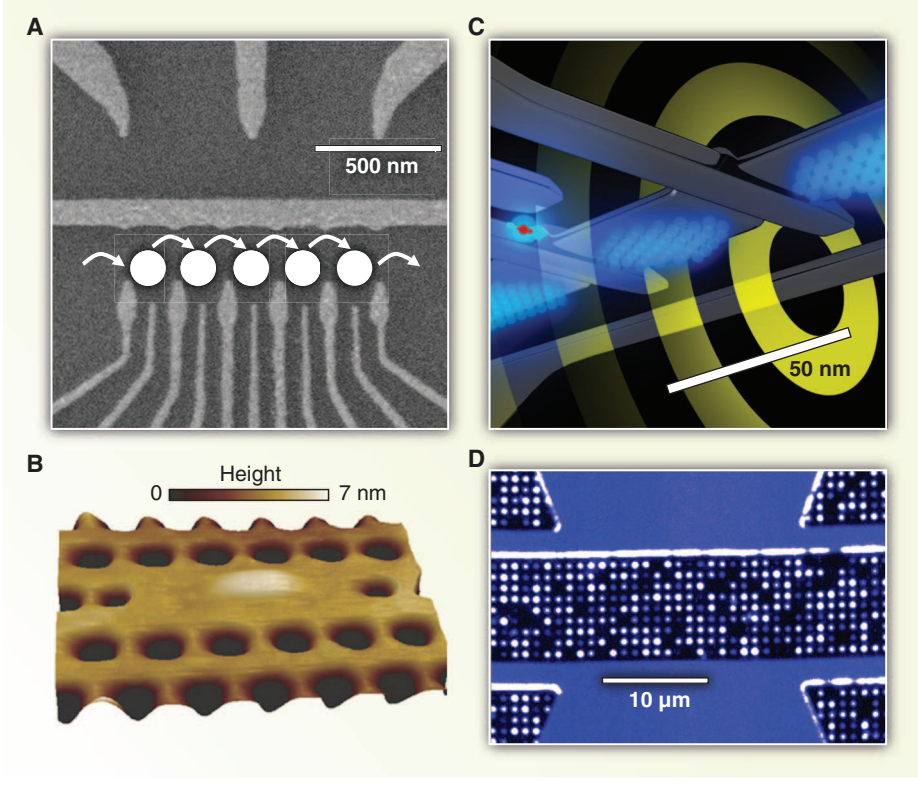

Fig. 2. Semiconductor qubit architectures. (**A**) Scanning electron microscope image of a gate-defined quintuple QD in a GaAs/AlGaAs heterostructure. Each QD is designed to contain one or two electron spins. (**B**) Atomic force microscope image of a single self-assembled InAs QD strongly coupled to a GaAs photonic crystal cavity, which is used to confine photons to small regions of space. Originally published in (*46*) and adapted with permission. (**C**) Schematic of a spin qubit device based on a single phosphorus dopant atom (red) implanted in silicon (*19*). The qubit electron spin is initialized and measured electronically through spin-dependent tunnel coupling to a nanofabricated single-electron transistor (gray) and manipulated using pulsed ac magnetic fields (yellow concentric circles) delivered by an integrated microwave transmission line. Image credit: W. Algar-Chuklin. (**D**) Confocal microscope image showing an array of implanted nitrogen vacancy centers in diamond aligned to a microwave transmission line. [Adapted with permission from (*61*); copyright (2010) American Chemical Society]

time, artificial atoms formed using gate electrodes in analogy with QDs in III/V heterostructures have also met with success (*18*). Coherent oscillations between two-electron singlet and triplet states of a double QD defined in a Si/SiGe heterostructure were demonstrated in 2012 (*23*), in direct analogy with experiments in III/V QDs (*21*). The measured dephasing time $T_2^* \approx 360$ ns was more than an order of magnitude longer than in GaAs thanks to the much weaker hyperfine coupling in natural silicon, and further improvements are expected for devices using isotopically enriched ^{28}Si.

Another group IV material with great promise for quantum information technology is diamond. With its large 5.5 eV band gap, diamond supports a plethora of optically active point defects, many of which are paramagnetic and could therefore serve as spin qubits. The most intensely studied of these is the nitrogen-vacancy (NV) center, consisting of a substitutional nitrogen atom adjacent to a vacancy in the diamond crystal. In its negatively charged ground state, the NV center is an electron spin triplet, and a special set of optical transitions facilitate the initialization and measurement of its spin state simply through optical excitation and fluorescence detection, respectively (*24*). Diamond's unique properties, particularly weak spin-orbit interactions, an extremely high Debye temperature (limiting spin-lattice relaxation), and the large band gap that energetically isolates interband electronic states, endow NV center spins with remarkable coherence properties that persist up to room temperature. Furthermore, isotopic purification of spin-free ^{12}C diamond leads to ultralong coherence times, up to several milliseconds at room temperature (*25*). With on-chip microwave-frequency waveguides enabling quantum control operations on subnanosecond time scales (*26*), more than one million coherent operations can be performed within the NV center's spin coherence time.

A key feature of NV center spin qubits is access not only to the electronic spin state but also to the individual nuclear spins of the intrinsic nitrogen atom and proximal ^{13}C nuclei (*27*). This makes each NV center a small "quantum register" consisting of several individually addressable nuclear spin qubits with exceptional coherence properties that can be initialized (*28*), measured nondestructively in a single shot (*29*), and even entangled (*30*) through their interactions with the electron spin. These nuclear spins could act as operational qubits in their own right, with the electron spins serving as ancillary qubits for initialization and readout, or as integrated quantum memory nodes associated with each electronic spin qubit. A room-temperature quantum memory consisting of a single ^{13}C nucleus weakly coupled to an NV center has been demonstrated with coherence exceeding 1 s (*31*). At temperatures $\lesssim$10 K, coherent optical transitions enable nondestructive single-shot spin measurements (*32*), coherent control (*33*), and spin-photon entanglement (*34*), with promise for integrating distributed NV center nodes within a large-scale optical network.

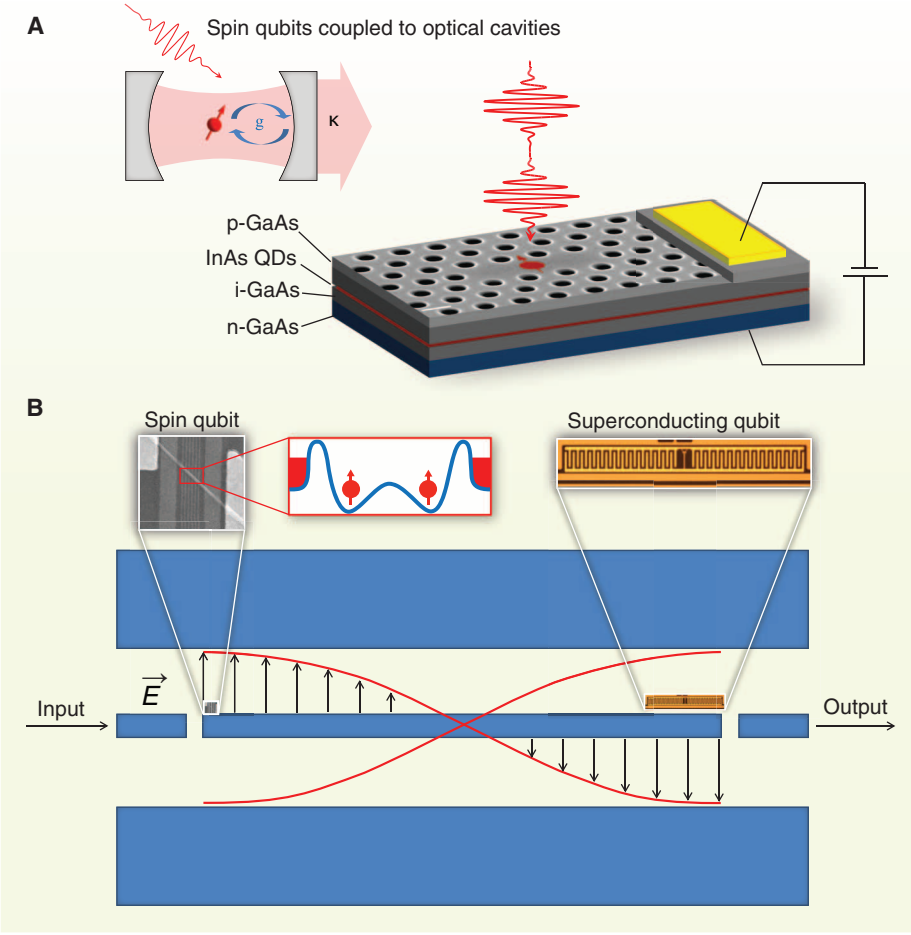

Fig. 3. (**A**) Cavity quantum electrodynamics with optical photons. (Upper left) Schematic of a single spin embedded within an optical cavity. If the qubit-cavity coupling strength, g, dominates over both qubit decoherence and the loss rate of photons from the cavity, κ, the system is in the strong coupling regime. (Lower right) Schematic of a photonic crystal cavity integrated with a diode structure used to realize coherent optical control of a cavity-coupled QD spin (*48*). [Image courtesy of D. Gammon, U.S. Naval Research Laboratory] (**B**) Superconducting qubits and spin qubits have quantum transitions in the microelectron volt range, closely matching the energy of microwave photons. This cartoon depicts a circuit quantum electrodynamics architecture that is used to couple a spin qubit to a superconducting qubit via a microwave cavity.

Scalable Architectures

With high-fidelity control of individual spin qubits now routine in many semiconductor systems, solid-state devices are poised to reach their full potential for integration and scalability. Nevertheless, a pressing challenge is the development of a robust two-qubit gate that can be scaled up to link many computational nodes into a larger network. One approach is to fabricate multiple qubits close enough together to use "direct" interactions such as magnetic dipole-dipole or electrostatic coupling to generate an entangling gate—for example, to implement a "surface code" computation using nearest-neighbor interactions only (*35*, *36*). This has been achieved both for pairs of lithographic quantum dot qubits in GaAs (*37*) and for NV center spins (*38*), although in both cases the gate time is rather long, limiting the entanglement fidelity. Furthermore, for applications in quantum communication and distributed quantum computing, it is desirable to be able to implement two-qubit gates between spins that are spatially separated beyond the reach of nearest-neighbor interactions. Such long-range coupling requires a "quantum bus" to transmit quantum information between local nodes. Although ideas exist for using nanomechanical resonators (*39*), "chains" of fixed spins (*40*), or electrons themselves carried by travelling QDs (*41*, *42*) as such a bus, an obvious choice of "flying qubit" to transmit information is the photon.

Photons are an excellent means of linking physical nodes within a network (*43*). They are capable of rapid propagation, low dissipation,

and low signal loss via integrated waveguides or fibers leading to or from the outside world. Furthermore, high-quality solid-state optical cavities mediate the coupling strength between spin qubits and photons (*44*), providing tools for photon-based selective readout and state preparation. When a qubit is optimally matched to an optical cavity—in the "strong coupling" regime (Fig. 3A)—the coherent interaction between the qubit and the cavity modes dominates over other, dissipative processes, such as the loss of photons from the cavity or the emission of qubit excitations to competing states. Notably, progress in the design and fabrication of dielectric optical cavities over the past decade has allowed the achievement of strong coupling between microcavities and semiconductor QDs (*45*, *46*). Strongly coupled systems produce entangled qubit-cavity states, such that the resulting photons carry the signature of the quantum state of the qubit, allowing long-distance propagation of that physical state information throughout the network. Although tremendous progress has been made in controlling purely photonic behavior with high-Q cavities and optically active QDs (*47*), it has remained a challenge to study cavity-coupled spin qubits. Promisingly, a photonic crystal cavity device integrated with a diode structure (Fig. 3A), necessary to tune the charge state of embedded QDs, has enabled coherent optical control of cavity-coupled spin qubits (*48*).

For "emerging" materials like diamond, where new fabrication techniques are required, cavity coupling to NV centers and other optical qubits still has much room for progress (*49*). Even without well-developed optical cavities, however, photons can still mediate coherent information transfer between distant qubits. A protocol has recently been developed to generate heralded entanglement between two NV center electron spins in separate cryostats 3 m apart (*50*). Using the dc Stark effect to tune the NV center optical transitions (*51*), a pair of indistinguishable photons is prepared, each entangled with their source NV center spins. By performing joint quantum measurements on the photons, the spin-photon entanglement is "swapped" to generate an entangled state of the two spins. Given the ability to initialize, measure, and entangle nuclear spin quantum registers local to each NV center (*28*–*30*), this protocol could enable long-distance quantum teleportation of spin states, quantum repeaters, and extended quantum networks.

Although optically active qubits such as self-assembled QDs and NV centers lend themselves naturally to photonic coupling, electronic qubits can also couple to photons, particularly those in the microwave regime. In fact, typical spin resonance frequencies of electronic spins in moderate magnetic fields are in the gigahertz range, closely matched to existing microwave resonator designs and even superconducting qubit architectures (*52*). A first step toward implementing "circuit quantum electrodynamics" with spin qubits was the recent demonstration of coupling between an InAs spin-orbit qubit and a superconducting resonator (*53*). Superconducting resonators have been effectively used to couple superconducting qubits that are separated by nearly a centimeter (*54*) and could similarly link semiconductor spins either to each other or to superconducting qubits (Fig. 3B).

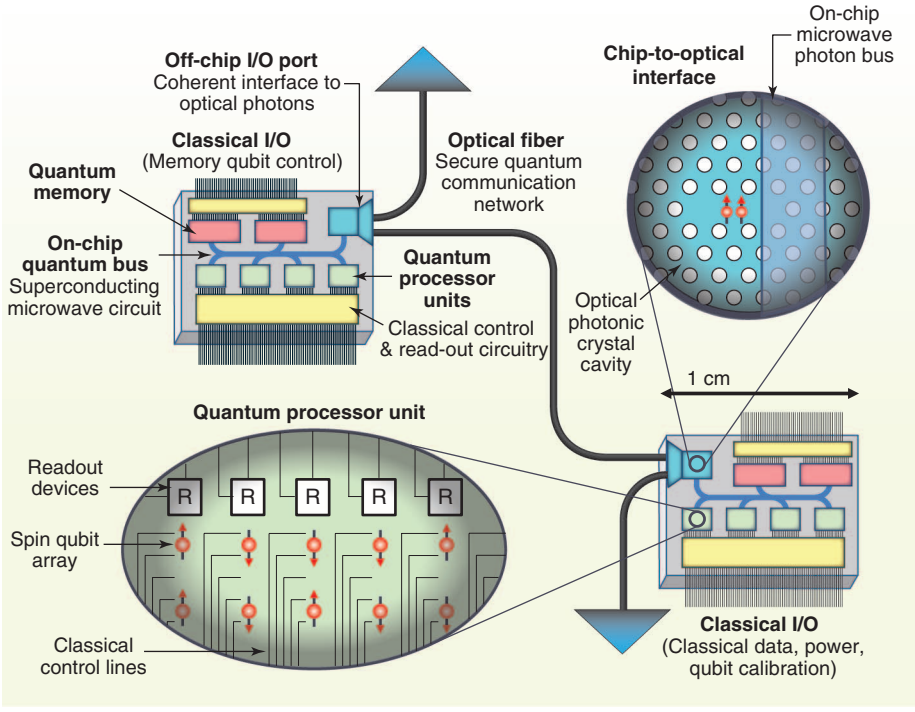

Fig. 4. A future integrated quantum device architecture might consist of quantum processor units comprising arrays of single-spin qubits, locally coupled on-chip using either photonic or microwave cavities. Photonic crystal cavities could be used to interface electron spins with optical photons, allowing long-distance transfer of quantum information via an optical fiber. Quantum memory might be located remotely from the processor units as depicted here or integrated with the processor qubits by using the nuclear spins of individual atoms. Classical circuitry provides qubit readout and calibration.

Outlook

It is tempting to view the wide array of systems under development as a race to find the "optimal" qubit, but this is likely to be the wrong perspective. Each implementation has relative strengths and weaknesses for different applications, and it could well serve to use each to its advantage. Modern computers comprise many types of logical implementations, including transistor logic, data transfer busses, and a large variety of memory nodes optimized either for fast access or long-term storage. A similar hybrid future could be in store for quantum computers, as envisaged in Fig. 4. Computational qubits will be chosen that are fast and easily coupled together, whereas memory nodes should be long lived but each need to be coupled to only one computational node. This might mean that the memory is not physically separated but is instead intrinsic to each computational node, being, for example, the nuclear spin of an NV center in diamond (*55*) or a phosphorus donor in silicon (*22*). Although optical interconnects are likely to serve as ports to transfer quantum information to and from the outside world, on-chip communication could be accomplished through either optical waveguides or superconducting microwave circuitry.

Although many challenges remain on the road to constructing a "useful" quantum computer, the pace of discovery seems to be accelerating, and spins in semiconductors are poised to play a major role. Several materials systems and architectures have already come to fruition, but others waiting in the wings might prove to be even better for some applications. For example, the remarkable properties of the diamond NV center motivates the search for other impurity-based spin systems with similar properties, possibly in more versatile host materials (*56*). Indeed, optically addressable defect spins with room-temperature coherence have recently been discovered in silicon carbide (*57*), which boasts well-developed techniques for heteroepitaxy and fabrication of complex structures. These and other material systems, such as rare-earth ions in crystals (*58*) and II/VI semiconductors (*59*), are likely to be a major focus in coming years.

The breadth of research in solid-state quantum information science is largely what makes the field so exciting. Advances achieved in one system are often directly applicable to many others, and solving the challenges that arise leads to breakthroughs that carry over to other fields of science and engineering. Clearly, the synergies between solid state and atomic physics are accelerating discoveries and demonstrations in both fields. Besides the potential we already recognize for quantum machines, our quest for greater control over quantum systems will surely lead to new materials and applications we have yet to imagine, just as the pioneers of classical computing could not have predicted exactly how the digital revolution has shaped our information age.

References and Notes

1. T. D. Ladd *et al.*, *Nature* **464**, 45 (2010).
2. R. Hanson, D. D. Awschalom, *Nature* **453**, 1043 (2008).
3. G. E. Moore, *Electronics* **38**, 114 (1965).
4. D. Loss, D. P. DiVincenzo, *Phys. Rev. A* **57**, 120 (1998).
5. R. Hanson, L. P. Kouwenhoven, J. R. Petta, S. Tarucha, L. M. K. Vandersypen, *Rev. Mod. Phys.* **79**, 1217 (2007).
6. J. R. Petta, H. Lu, A. C. Gossard, *Science* **327**, 669 (2010).
7. S. Nadj-Perge, S. M. Frolov, E. P. A. M. Bakkers, L. P. Kouwenhoven, *Nature* **468**, 1084 (2010).
8. J. Berezovsky, M. H. Mikkelsen, N. G. Stoltz, L. A. Coldren, D. D. Awschalom, *Science* **320**, 349 (2008).
9. D. Press, T. D. Ladd, B. Zhang, Y. Yamamoto, *Nature* **456**, 218 (2008).
10. W. B. Gao, P. Fallahi, E. Togan, J. Miguel-Sanchez, A. Imamoglu, *Nature* **491**, 426 (2012).
11. K. De Greve *et al.*, *Nature* **491**, 421 (2012).
12. G. de Lange, Z. H. Wang, D. Ristè, V. V. Dobrovitski, R. Hanson, *Science* **330**, 60 (2010).
13. C. A. Ryan, J. S. Hodges, D. G. Cory, *Phys. Rev. Lett.* **105**, 200402 (2010).
14. H. Bluhm *et al.*, *Nat. Phys.* **7**, 109 (2011).
15. A. M. Tyryshkin *et al.*, *Nat. Mater.* **11**, 143 (2011).
16. M. Steger *et al.*, *Science* **336**, 1280 (2012).
17. B. E. Kane, *Nature* **393**, 133 (1998).
18. J. J. L. Morton, D. R. McCamey, M. A. Eriksson, S. A. Lyon, *Nature* **479**, 345 (2011).
19. J. J. Pla *et al.*, *Nature* **489**, 541 (2012).
20. A. Morello *et al.*, *Nature* **467**, 687 (2010).
21. J. R. Petta *et al.*, *Science* **309**, 2180 (2005).
22. J. J. Pla *et al.*, http://arxiv.org/abs/1302.0047.
23. B. M. Maune *et al.*, *Nature* **481**, 344 (2012).
24. F. Jelezko, T. Gaebel, I. Popa, A. Gruber, J. Wrachtrup, *Phys. Rev. Lett.* **92**, 076401 (2004).
25. G. Balasubramanian *et al.*, *Nat. Mater.* **8**, 383 (2009).
26. G. D. Fuchs, V. V. Dobrovitski, D. M. Toyli, F. J. Heremans, D. D. Awschalom, *Science* **326**, 1520 (2009).
27. L. Childress *et al.*, *Science* **314**, 281 (2006).
28. M. V. G. Dutt *et al.*, *Science* **316**, 1312 (2007).
29. P. Neumann *et al.*, *Science* **329**, 542 (2010).
30. W. Pfaff *et al.*, *Nat. Phys.* **9**, 29 (2013).
31. P. C. Maurer *et al.*, *Science* **336**, 1283 (2012).
32. L. Robledo *et al.*, *Nature* **477**, 574 (2011).
33. B. B. Buckley, G. D. Fuchs, L. C. Bassett, D. D. Awschalom, *Science* **330**, 1212 (2010).
34. E. Togan *et al.*, *Nature* **466**, 730 (2010).
35. L. Trifunovic *et al.*, *Phys. Rev. X* **2**, 011006 (2012).
36. R. Raussendorf, J. Harrington, *Phys. Rev. Lett.* **98**, 190504 (2007).
37. M. D. Shulman *et al.*, *Science* **336**, 202 (2012).
38. F. Dolde *et al.*, http://arxiv.org/abs/1212.2804 (2012).
39. P. Rabl *et al.*, *Nat. Phys.* **6**, 602 (2010).
40. S. Bose, *Contemp. Phys.* **48**, 13 (2007).
41. R. P. G. McNeil *et al.*, *Nature* **477**, 439 (2011).
42. S. Hermelin *et al.*, *Nature* **477**, 435 (2011).
43. H. J. Kimble, *Nature* **453**, 1023 (2008).
44. K. J. Vahala, *Nature* **424**, 839 (2003).
45. J. P. Reithmaier *et al.*, *Nature* **432**, 197 (2004).
46. K. Hennessy *et al.*, *Nature* **445**, 896 (2007).
47. I. Fushman *et al.*, *Science* **320**, 769 (2008).
48. S. G. Carter *et al.*, http://arxiv.org/abs/1211.4540 (2012).
49. I. Aharonovich, A. D. Greentree, S. Prawer, *Nat. Photonics* **5**, 397 (2011).
50. H. Bernien *et al.*, http://arxiv.org/abs/1212.6136 (2012).
51. L. C. Bassett, F. J. Heremans, C. G. Yale, B. B. Buckley, D. D. Awschalom, *Phys. Rev. Lett.* **107**, 266403 (2011).
52. A. Wallraff *et al.*, *Nature* **431**, 162 (2004).
53. K. D. Petersson *et al.*, *Nature* **490**, 380 (2012).
54. L. DiCarlo *et al.*, *Nature* **467**, 574 (2010).
55. G. D. Fuchs, G. Burkard, P. V. Klimov, D. D. Awschalom, *Nat. Phys.* **7**, 789 (2011).
56. J. R. Weber *et al.*, *Proc. Natl. Acad. Sci. U.S.A.* **107**, 8513 (2010).
57. W. F. Koehl, B. B. Buckley, F. J. Heremans, G. Calusine, D. D. Awschalom, *Nature* **479**, 84 (2011).
58. R. Kolesov *et al.*, http://arxiv.org/abs/1301.5215 (2013).
59. T. D. Ladd, K. Sanaka, Y. Yamamoto, A. Pawlis, K. Lischka, *Phys. Status Solidi B* **247**, 1543 (2010).
60. G. D. Fuchs *et al.*, *Nat. Phys.* **6**, 668 (2010).
61. D. M. Toyli, C. D. Weis, G. D. Fuchs, T. Schenkel, D. D. Awschalom, *Nano Lett.* **10**, 3168 (2010).

Acknowledgments: D.D.A., L.C.B., and E.L.H. acknowledge support from the Air Force Office of Scientific Research and the Defense Advanced Research Projects Agency (DARPA); A.S.D. from the Australian Research Council (project CE11E0096) and the U.S. Army Research Office (contract W911NF-08-1-0527); and J.R.P. from the Sloan and Packard Foundations, Army Research Office grant W911NF-08-1-0189, NSF grants DMR-0819860 and DMR-0846341, and DARPA QuEST grant HR0011-09-1-0007.

10.1126/science.1231364

REVIEW

Topological Quantum Computation—From Basic Concepts to First Experiments

Ady Stern[1]* and Netanel H. Lindner[2,3]

Quantum computation requires controlled engineering of quantum states to perform tasks that go beyond those possible with classical computers. Topological quantum computation aims to achieve this goal by using non-Abelian quantum phases of matter. Such phases allow for quantum information to be stored and manipulated in a nonlocal manner, which protects it from imperfections in the implemented protocols and from interactions with the environment. Recently, substantial progress in this field has been made on both theoretical and experimental fronts. We review the basic concepts of non-Abelian phases and their topologically protected use in quantum information processing tasks. We discuss different possible realizations of these concepts in experimentally available solid-state systems, including systems hosting Majorana fermions, their recently proposed fractional counterparts, and non-Abelian quantum Hall states.

The principal obstacles on the road to quantum computing are noise and decoherence. By noise, we mean imperfections in the execution of the operations on the qubits (quantum bits). Decoherence arises when the quantum system that encodes the qubits becomes entangled with its environment, which is a bigger, uncontrolled system. There are two approaches to tackling these barriers. One is based on complete isolation of the computer from its environment, careful elimination of noise, and protocols for quantum correction of unavoidable errors. Enormous progress has been achieved in this direction in the past few years. The other approach, which is at the root of topological quantum computation, is very different. It uses a non-Abelian state of matter (*1*–*10*) to encode and manipulate quantum information in a nonlocal manner. This nonlocality endows the information with immunity to the effects of noise and decoherence (*2*–*6*).

Non-Abelian States of Matter

Several properties define a non-Abelian state of matter (*1*, *2*, *6*–*10*). It is a quantum system whose

[1]Department of Condensed Matter Physics, Weizmann Institute of Science, Rehovot 76100, Israel. [2]Institute of Quantum Information and Matter, California Institute of Technology, Pasadena, CA 91125, USA. [3]Department of Physics, California Institute of Technology, Pasadena, CA 91125, USA.

*To whom correspondence should be addressed. E-mail: adiel.stern@weizmann.ac.il

ground state is separated from the excited part of the spectrum by an energy gap. The elementary particles of the system may form collective composite particles, known as "non-Abelian anyons." When that occurs, the ground state becomes degenerate. In the limit of a large number of anyons, N, the ground-state degeneracy is λ^N, and the anyon is said to have a "quantum dimension" of λ. This degeneracy is not a result of any obvious symmetry of the system. As such, it is robust and cannot be lifted with the application of any local perturbation (*11*).

Transformations between the degenerate ground states may be induced by exchanging the anyons' positions. The canonical example is that of a two-dimensional (2D) system, where anyons may be regarded as point particles. Imagine a set of anyons that are initially positioned on a plane at $(R_1 \ldots R_N)$. They are made to move along a set of trajectories $[R_1(t) \ldots R_N(t)]$ that ends with their positions permuted. The motion is slow enough not to excite the system out of the subspace of ground states. When viewed in a 3D plot, the set of trajectories, known also as world lines, $R_i(t)$ look like entangled strands of spaghetti. A "braid" is defined as a set of spaghetti configurations that can be deformed to one another without spaghetti strands being cut. Remarkably, the unitary transformation implemented by the motion of the anyons depends only on the braid and is independent of the details of the trajectories. These unitary transformations must satisfy a set of conditions that result from their topological nature, such as the Yang-Baxter equation (Fig. 1A).

Notably, for the braid in which two anyons of types a and b are encircled by a third that is far away (Fig. 1B), the corresponding transformation will not be able to resolve the two anyons' types; from a distance they would look as if they "fused" to one anyon, of type c. The fusion of a pair of non-Abelian anyons may result in several different outcomes that are degenerate in energy when the anyons are far away from one another (leading to the ground-state degeneracy). The degeneracy is split when the fused anyons get close. The list of cs to which any a-b pair may fuse constitutes the "fusion rules." For each anyon of type a, there is an "anti-anyon" $\bar{a}$ such that the two may annihilate one another, or be created as a pair.

Topological Quantum Computation

The properties of non-Abelian states that are important for our discussion are the quantum dimensions of the anyons, the unitary transformations that they generate by braiding, and their fusion rules. Different non-Abelian systems differ in these properties. To turn a non-Abelian system into a quantum computer, we first create pairs of anyons and anti-anyons from the "vacuum," the state of zero anyons. In the simplest computational model, a qubit is composed of a group of several anyons, and its two states, $|0\rangle$ and $|1\rangle$, are two possible fusion outcomes of these anyons. (A qudit is formed if there are more than two possible fusion outcomes.) The creation from the vacuum initializes qubits in a well-defined state. The unitary gates are implemented by the braid transformations (Fig. 1C). At the end of the computation, the state is read off by measuring the fusion outcome of the anyons (*2*–*6*).

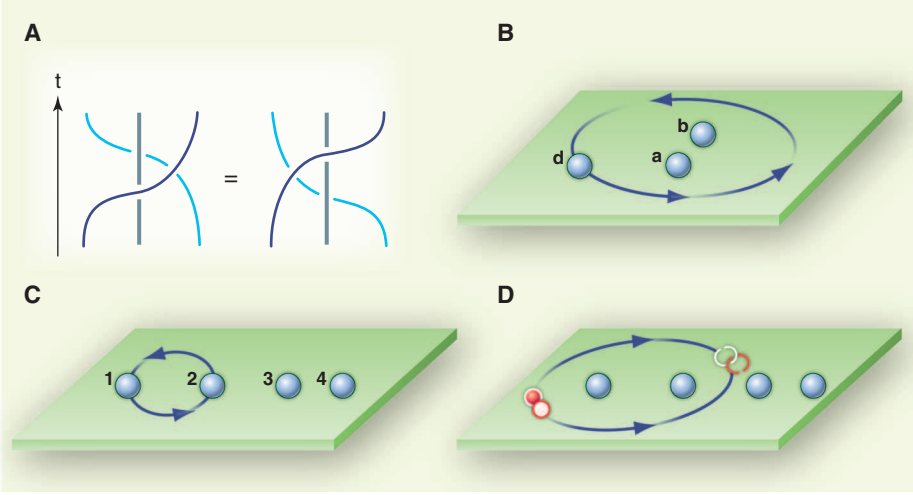

Fig. 1. (**A**) The Yang-Baxter equation states that two exchange paths that can be deformed into each other without cutting the world lines of the particles (blue curves) define the same braid. (**B**) Two anyons labeled a and b are encircled by a third anyon d. The resulting transformation depends only on the fusion outcome of a and b. (**C**) A canonical construction for a qubit, in a system of Ising anyons, consists of four anyons that together fuse to the vacuum. The two possible states can then be labeled by the fusion charge, say, of the left pair. A single qubit $\pi/4$ gate can be used by exchanging anyons 1 and 2 (depicted), whereas a Hadamard gate can be used by exchanging anyons 2 and 3. Such a construction can be realized using Majorana fermions. (**D**) Decoherence of information encoded in the ground-state space. Thermal and quantum fluctuations nucleate a quasiparticle-antiquasiparticle pair (red, white). The pair encircles two anyons encoding quantum information, and annihilates. The result of the process depends on the fusion charge of the two anyons, leading to decoherence of the encoded quantum information.

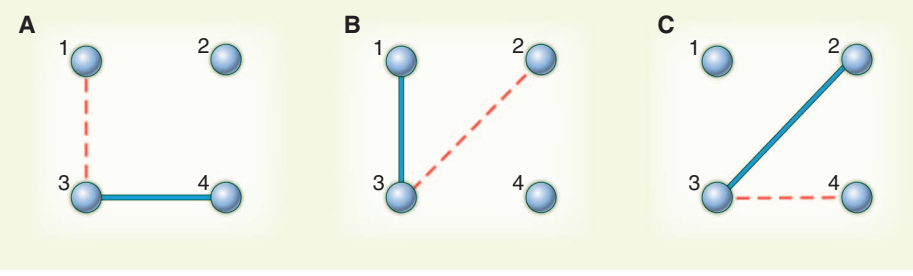

Fig. 2. Braiding in a system hosting Majorana fermions (zero modes or their fractionalized counterparts). For a manipulation of the subspace of ground states to lead to a topological result, the number of ground states should remain fixed. (**A**) Two zero modes initially at locations 1 and 2 are to be interchanged. A pair of coupled zero modes, 3 and 4, is created from the vacuum and may reside, for example, at the two ends of a short wire. As long as 3 and 4 are coupled (blue line), they are not zero modes and do not change the degeneracy of the ground state. Next, location 1 is coupled to 3 and 4 (red dashed line). The coupled system of 1, 3, and 4 must still harbor a zero mode. Thus, this step does not vary the degeneracy of the ground state, but it does redistribute the wave function of that zero mode among the three coupled sites. Location 4 is then decoupled from 1 and 3, and the localized zero mode is now at location 4. The outcome is then that 1 was copied to location 4. (**B**) In a similar fashion, 2 is copied to location 1. (**C**) Finally, 1 is copied from location 4 to location 2. At the end of this series, 3 and 4 are again coupled to one another, but 1 and 2 have been interchanged.

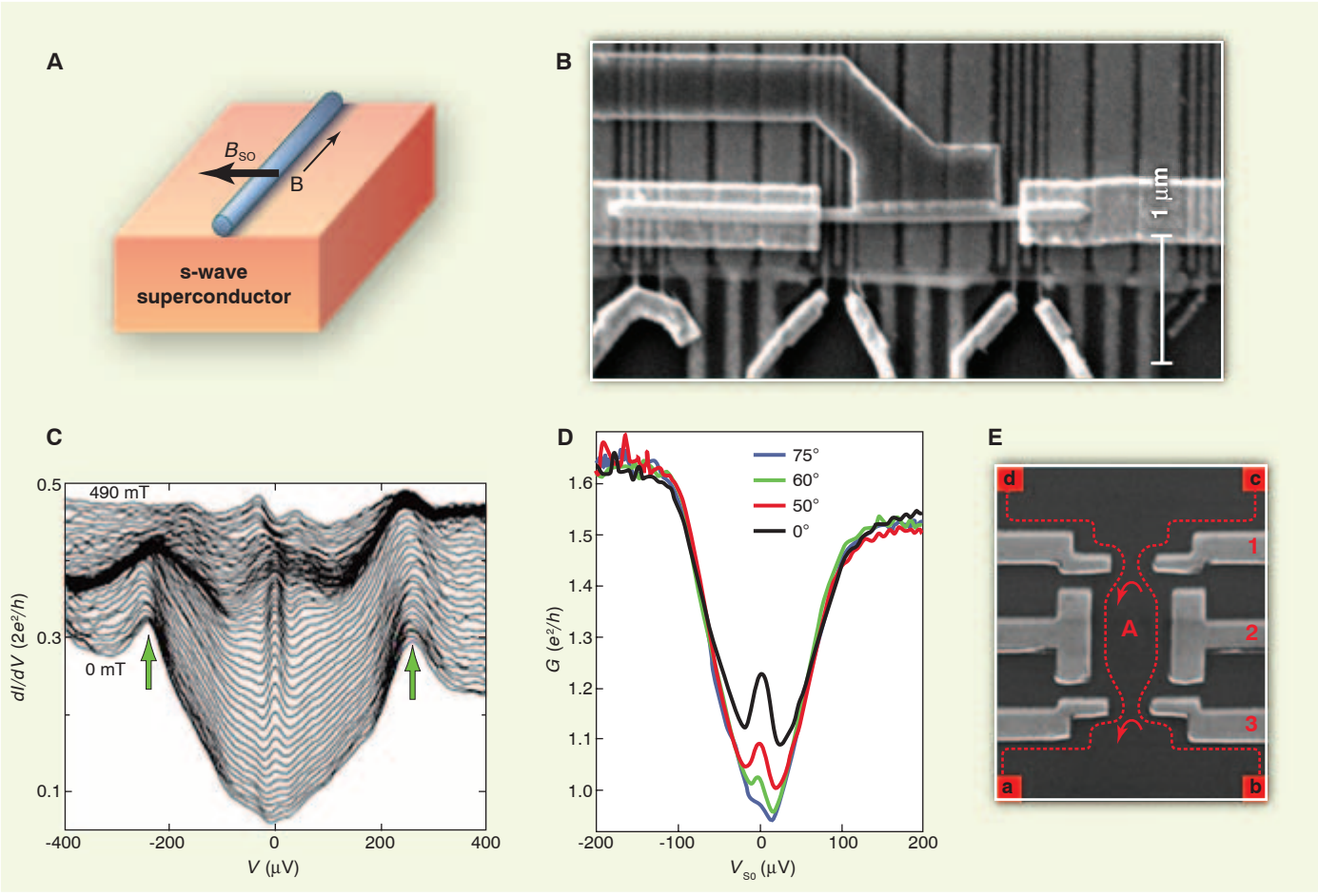

Fig. 3. Majorana end modes in a quantum wire. (**A**) A schematic plot of the sample: a quantum wire lying on a superconductor. B is the magnetic field that couples to the electron's spin, and B_{so} is the effective magnetic field induced by spin-orbit scattering. (**B**) A picture of the sample. Scale bar, 1 μm. (**C** and **D**) The measured differential conductance as a function of voltage at a range of magnetic fields (C) and magnetic field orientation (D) in the experiments reported in (*28*) and (*29*), respectively. The peak at zero voltage may be a sign of a Majorana fermion zero mode. (**E**) The experimental device of the type used in (*50*, *58*) to measure interference of quasiparticles in the ν = 5/2 state. The periodicity of the interference pattern as a function of magnetic field and gate voltage reflects the non-Abelian nature of the quasiparticles (*54*–*56*). Indicated are the interference loop (A), the interfering trajectories (dashed lines), ohmic contacts (a to d), and gates (numbered). [(A), (B), and (C) reprinted from (*28*); (D) reprinted from (*29*) by permission of Macmillan Publishers Ltd., copyright 2012; (E) reprinted from (*58*)]

The process outlined above is immune to noise and decoherence. The only mechanism that may alter the quantum state of the qubit in an uncontrolled fashion is a quantum or thermal fluctuation that creates an anyon–anti-anyon pair from the vacuum; the pair braids around two of the qubit's anyons, and finally annihilates (Fig. 1D). The probability for such a process decreases exponentially with decreasing temperature and with increasing distance between the anyons.

A quantum computer needs to have a minimal set of gates that allow it to efficiently approximate any unitary transformation in its space of logical states. Such a set is commonly called universal (*12*, *13*). For example, a universal set may be composed of two single-qubit gates and a two-qubit controlled-not gate (CNOT). For some non-Abelian states, all of these gates may be carried out in a topologically protected way (*2*, *4*–*6*). Fortunately, even when that is not the case, universality may still be obtained by combining topological and nontopological operations, as shown below (*14*, *15*).

Zero Modes and Majorana Fermions

A useful concept for understanding the stability of the degeneracy of the ground state in non-Abelian systems is that of localized "zero modes" (*16*, *17*). These are operators that act only within the subspace of ground states, and whose operation is confined to a localized spatial region. Generally, the number of independent operators that transfer the system between orthogonal ground states must be even. Thus, when there is only one such operator acting within a given spatial region, it must be Hermitian (note that Hermitian conjugation does not change the location of the operator). Consequently, it must have a partner in a different spatial region. If the system is subjected to a perturbation that acts locally within one of the regions, the local zero mode cannot be eliminated, because its partner is not subjected to that perturbation.

The position and wave function of the zero modes depend on the parameters of the system. Braiding operations are carried out by a cyclic trajectory in this parameter space. The braiding of world lines in two dimensions (*18*, *19*) is a particular example of topologically distinct classes of cyclic trajectories in the parameter space. More generally, the unitary transformation applied by a cycle is determined by the topological class to which the cycle belongs. This allows for braiding operations in systems that are not 2D, such as networks of 1D wires (*20*–*22*) (Fig. 2).

The simplest non-Abelian states of matter, those that carry Majorana fermions (*16*, *17*), can

be explained using the concept of zero modes. Such systems usually combine spin-orbit coupling, superconductivity, and Zeeman coupling to the electron spin (*23*–*27*). In superconductors, operators that take the system from one energy state to another are superpositions of electron creation and annihilation operators. In certain conditions, localized zero modes occur, in which the amplitude for the creation and annihilation operators is equal in magnitude, and the resulting operator is Hermitian. These operators are commonly referred to as Majorana fermions. The non-Abelian state of matter occurs when the zero modes are spatially separated from one another. Like all zero modes, Majorana fermions occur in pairs. A pair of Majorana fermions form a complex conventional fermion that spans a Hilbert space of two dimensions. The quantum dimension of a single Majorana fermion is therefore $\sqrt{2}$.

Because a superconductor is gapped, Majorana fermions in a superconducting system can only occur where the superconducting gap closes locally. In 2D systems, Majorana fermions are to be found in vortex cores (*16*, *18*), whereas in 1D systems they are to be found at the interfaces between different types of superconductivity, or at the system's ends (*17*). In vortex cores of s-wave superconductors, the presence of two spin directions per each electronic state does not allow for an isolated Majorana fermion zero mode. The places to look for isolated Majorana fermions are superconductors with only one spin direction per each electronic state. Examples are superconductors with spin-polarized p-wave pairing (*16*, *17*), surfaces of 3D and edges of 2D topological insulators (*23*, *24*), and 2D/1D systems featuring both spin-orbit and Zeeman couplings (*25*–*27*) in proximity to superconductors.

Recent experiments (*28*–*32*) support the existence of Majorana fermions at the ends of semiconducting wires in which strong spin-orbit coupling, together with Zeeman coupling of the spin to a magnetic field, creates a range of densities at which spin degeneracy is removed. The wires are made superconducting through their proximity to a superconductor, and zero modes are expected to form at their ends, which are separated from metallic contacts by potential barriers. When a current is driven through the wires in the absence of the end modes, the combination of the barriers and the superconducting gap suppresses the current at low voltages. The Majorana end modes allow current to flow, resulting in a sharp peak in the wires' differential conductance at zero voltage. This peak was observed in several experiments (Fig. 3) and its characteristics are consistent with Majorana end modes in quantum wires.

Although these are encouraging observations, it is still too early to identify them unambiguously as originating from Majorana fermions. The wires used in the experiments were short enough that coupling between the two ends may be expected to split the degeneracy between the end modes. Future experiments may observe the decay of this splitting with increasing wire length. Different measurements using the Josephson effect, Coulomb blockade, and scanning tunneling microscopes may provide additional information.

The Majorana fermions on the ends of quantum wires offer useful insights into the physics of non-Abelian systems. In the absence of the Majorana fermions, the ground state of a clean superconducting wire has an even number of electrons paired to Cooper pairs. Adding another electron is costly in energy, because this electron has no pairing partner. When the two Majorana fermions are localized at the ends of the wire, the odd electron can join at no cost of energy. The two degenerate ground states are then of different electron parities. When there are N wires, there are $2N$ zero modes and 2^N states, with each wire having either an even or odd number of electrons. This manner of counting explains the quantum dimension of $\sqrt{2}$.

Magic State Distillation and Surface Codes

Majorana fermions realize fusion and braiding rules analogous to those of "Ising anyons." Interchanging Majorana fermions at the ends of the same wire is equivalent to rotating the wire; this preserves the parity of the electron number while implementing a relative phase shift of $\pi/2$ between states of different parities. The braiding of two Majorana fermions of two different wires (Fig. 2) leads to a unitary transformation that takes the two wires from a state of well-defined parities to a state that is a superposition of even and odd parities, with equal probabilities. For example, the state $|\text{even1,even2}\rangle$ is transformed to the state $1/\sqrt{2}$ [$|\text{even1,even2}\rangle \pm i|\text{odd1,odd2}\rangle$], where the sign of the second term depends on the details of the interchange. Because only two types of interchanges are possible—intrawire and interwire—there is no topologically protected way to turn two wires that start, say, at even parities $|\text{even1,even2}\rangle$ into an arbitrary superposition of the

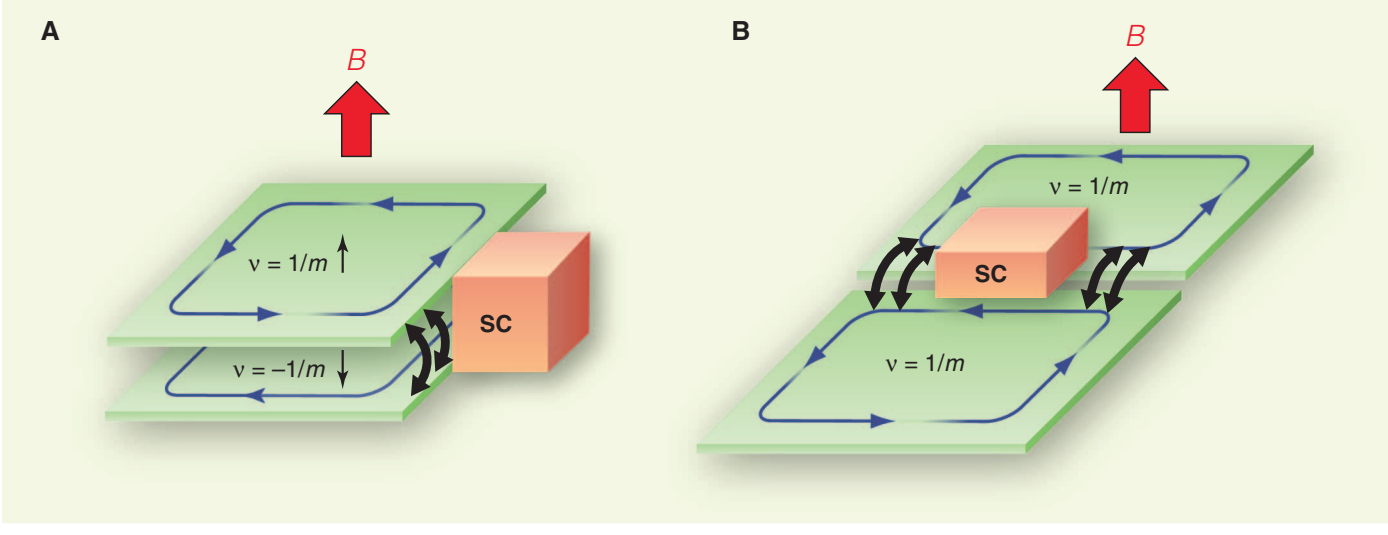

Fig. 4. Fractionalized Majorana zero modes at the interface between the superconductor and tunneling regions. (**A**) An electron-hole bilayer where the two layers are in a FQHE where the Hall conductivities are quantized at $\nu = \pm 1/m$ (in units of e^2/h), where m is an odd integer. The direction of the edge modes is indicated by the blue arrows. An s-wave superconductor (SC; orange) coupled to the edge of the two-layer system can gap the edge modes. In nonsuperconducting regions, spin-flipping electron tunneling between the top and bottom layer (black arrows) opens a gap on the edge. These can be enhanced by coupling the edge to a ferromagnet. Two layers of graphene may be a possible realization for such a system. (**B**) Single-layer realization, with a trench cut in a FQHE state with $\nu = 1/m$ exposing counterpropagating edge states. In spin-polarized quantum Hall states, spin-orbit interaction would couple these modes to a superconductor.

type $a|\text{even1,even2}\rangle \pm b|\text{odd1,odd2}\rangle$, with $|a| \neq |b|$. Topological quantum computation with Majorana fermions is therefore not universal (*4*–*6*). Using topologically protected braiding and measurement operations, Majorana fermions may carry out a set of gates known as the "Clifford gates." This set is generated by the single-qubit Hadamard gate, the single-qubit Pauli matrices, and the two-qubit CNOT gate (the latter requires a parity measurement of two qubits) (*13*). The gap to universal quantum computation may be bridged by adding a single-qubit gate that rotates the qubit by an angle $\pi/8$ (values other than $\pi/8$ are also possible).

Although topologically protected operations cannot implement the missing gate, they are able to approximate this gate with an arbitrarily small error, using a protocol called "magic state distillation" (*14*, *15*). The protocol consists of three key steps. First, nontopological operations create a large number of resource qubits in a "noisy" version of the state $|\psi_M\rangle = 1/\sqrt{2}\,[|0\rangle + \exp(i\pi/4)|1\rangle]$. [Note that there is no known way to accurately create the state $|\psi_M\rangle$ by using Clifford gates (i.e., topologically protected operations) alone.]

In the second step, one almost accurate qubit in the state $|\psi_M\rangle$ is distilled, using only topologically protected operations, from a large number of the noisy resource states. The possibility to do this endows $|\psi_M\rangle$ with the affectionate name "magic state." The distillation protocol is based on the concept of a "stabilizer" quantum error-correcting code (*33*). A quantum error-correcting code uses n physical qubits that span a space of 2^n states to represent one logical qubit. A unitary transformation takes a state of a single "logical" qubit and encodes it in this 2^n-dimensional space. As long as only a limited number of errors occur in the encoded state, they may be detected and corrected by measurements carried out on the n-qubit system, without disturbing the encoded quantum information.

In a stabilizer code, Pauli measurements and Clifford operations are sufficient for information encoding, decoding, and error correction. In the particular stabilizer code used for magic state distillation, Clifford operations can transform n qubits in the state $|\psi_M\rangle$ to an encoded logical state. Therefore, this code can be used to take n of the qubits that are noisy yet close enough to the state $|\psi_M\rangle$, encode them, detect the errors in their combined n-qubit state, keep only the error-free instances, and decode back to a single-qubit state. This entire step may be done in a topologically protected manner. Because the number of detectable errors is limited, this procedure cannot yield perfect magic states. However, the output is closer to the desired $|\psi_M\rangle$ than are the input resource states. This step can be applied repeatedly until the required level of accuracy is reached.

In the third and final step, the distilled magic states are used as ancillary qubits in order to apply the single-qubit rotation that is missing in the Clifford gates set. This is accomplished by measuring the joint parity of the logical qubit and the ancilla in the state $|\psi_M\rangle$. If the initial state of the logical qubit is $\alpha|0\rangle + \beta|1\rangle$, the measurement entangles the qubit and the ancilla either to the state $1/\sqrt{2}\,[\alpha|00\rangle + \beta \exp(i\pi/4)|11\rangle]$ or to $1/\sqrt{2}\,[\exp(i\pi/4)\alpha|01\rangle + \beta|10\rangle]$, depending on its outcome. A CNOT operation then disentangles the qubit from the ancilla, resulting in the required operation on the logical qubit. Magic state distillation complements the set of Clifford gates and opens the way to universal quantum computation based on Majorana fermions. The optimization of distillation protocols is currently under study (*34*).

In any physical realization of topological quantum computing, we must still expect an inevitable amount of errors. A promising approach for dealing with these errors is to incorporate topological qubits into a particularly fault-tolerant class of stabilizer codes, known as "surface codes." These codes consist of a 2D or 3D array of qubits (*3*, *35*). In surface codes, the states used to encode the logical qubit are the ground states of a Hamiltonian that describes couplings between different physical qubits in the array. This Hamiltonian gives rise to Abelian anyons. Two Abelian anyons have only one fusion outcome and therefore do not have the full advantages of their non-Abelian counterparts. Nonetheless, the surface codes do offer an enhanced robustness to decoherence and noise. The logical quantum information is encoded by the presence or absence of Abelian anyons on holes cut out in the array. An error occurring in a surface code amounts to creating an excited anyon–anti-anyon pair, which can be located and corrected by performing Pauli measurements and Clifford operations on the code's qubits. The error tolerance of surface codes can be several orders of magnitude better than most other known types of quantum error-correcting codes, but it comes at the price of the large number of physical qubits needed to encode a single logical qubit.

The ideas outlined above have inspired several proposals for hybrid structures of topological and nontopological components. These structures either combine nonprotected superconducting qubits or charge qubits with protected Majorana qubits, or combine protected quantum Hall interferometric gates with nonprotected parts (*36*–*41*). The role of the nontopological parts is limited to the operations that cannot be carried out in a protected manner, requiring effective and fast control of the coupling of the nontopological and topological parts.

Non-Abelian Anyons in Quantum Hall Systems

Non-Abelian anyons with properties richer than those of Majorana fermions are known in several systems. Below, we survey non-Abelian anyons on the edges of Abelian quantum Hall systems (*42*–*47*) and non-Abelian quantum Hall states (*1*, *2*, *10*, *16*, *48*).

The 2D gapped bulk of the quantum Hall effect is accompanied by 1D gapless edge modes. These modes occur at the interface of a quantum Hall state with the vacuum, between quantum Hall states of different filling factors, or even between quantum Hall states of the same filling factor and different spin polarization. We focus here on cases where gapless modes flow in both directions; these modes may be gapped by a perturbation that induces backscattering between them. One such case (Fig. 4A) is bilayer electron-hole system, in which the electrons and the holes are subjected to the same magnetic field and have the same densities. Because of their opposite charges, the two layers carry counterpropagating edge modes in physical proximity. When the values of the quantized Hall conductivities at the two layers (in units of e^2/h) are $\nu = \pm 1/m$, there is one mode flowing in each of the layers; in more complicated cases, there may be several such modes. Counterpropagating edge modes can also be realized in single-layer systems (Fig. 4B).

For $\nu = \pm 1/m$, the two counterpropagating edge modes may be gapped when they are both coupled either to a superconductor or to a ferromagnet (Fig. 4). In the two-layer case, the superconductor exchanges pairs of electrons with the two layers, one electron with each layer, whereas the ferromagnet scatters an electron from one layer to the other. In more complicated cases, there may be other ways to gap the edges, even with no superconductivity present. If different regions of the edge are gapped by different mechanisms, zero modes may appear at the interfaces between these regions. For $m = 1$, these are Majorana fermion zero modes, with quantum dimension $\sqrt{2}$. For the fractional case $m > 1$, the emerging anyons have a larger quantum dimension of $\sqrt{2m}$. In these cases, the regions on the edge that are coupled to superconductors form "superconducting quantum wires" and are otherwise surrounded by an insulating bulk. Their charge is then quantized modulo the charge of a Cooper pair. The quantization unit is the elementary charge of the surrounding medium, which is $1/m$ of the electron charge, resulting in $2m$ possible charge values.

The non-Abelian anyons that are realized on the gapped edges of Abelian quantum Hall systems may be braided using operations of the form outlined in Fig. 2. The unitary transformations that are realized by such braiding are richer than those realized by Majorana fermions. Unfortunately, these systems do not allow for universal quantum computation; however, they are robust to electronic noise and allow all Clifford operations to be performed using braiding. The precise computational potential of the non-Abelian anyons on edges of Abelian quantum Hall states has not yet been fully explored (*47*).

With respect to universal quantum computation, the most powerful anyons may be realized in the fractional quantum Hall effect (FQHE), in particular for states in the Landau level range of $2 < \nu < 4$. The non-Abelian anyons

in this system are fractionally charged quasiparticles. Despite the differences between these and the systems described above in the context of Majorana fermions, there are similarities in the path that may lead to the formation of non-Abelian anyons. In both systems, the interaction between electrons leads to states that may be viewed as a Bose-Einstein condensate. For superconductors, the condensed particles are Cooper pairs composed of two electrons each. For non-Abelian FQHE states, the condensed bosons are clusters of k electrons, with $k + 2$ magnetic flux quanta attached. The attached flux transmutes the electrons into Abelian anyons, and k of these anyons form the boson that condenses. The resulting state is a candidate state for Landau level fillings of $\nu = L + [2/(k + 2)]$ and $\nu = L + [k/(k + 2)]$, where L is the number of filled inert Landau levels. On the basis of numerical analysis, the most likely range of fillings where these states may be energetically favorable to other states has $L = 2$. These states are usually referred to as the Moore-Read state (for $k = 2$) (*1*) and the Read-Rezayi states (for $k \geq 3$) (*48*).

Similar to Majorana fermions, Moore-Read non-Abelian quasiparticles (*1*) have the quantum dimension of $\sqrt{2}$. For the Read-Rezayi states, the fractional statistics of the k anyons makes the counting of the ground states quite complicated. Briefly, the quantum dimension of the resulting non-Abelian anyons is $2\cos[\pi/(k + 2)]$, which is not a square root of an integer. The transformations implemented when the non-Abelian anyons of $k \neq 2$ or 4 are braided are rich enough to enable a universal set of quantum gates.

Numerical and experimental evidence (Fig. 3E) supports the identification of the $\nu = 5/2$ state as a Moore-Read state (*49*–*52*). Experimental investigation of states with $k \geq 3$ has so far been hindered by their fragility, reflected in a small energy gap and strong sensitivity to disorder.

The non-Abelian anyons realized by fractionally charged quasiparticles in FQHE states are full-fledged quantum dynamical degrees of freedom, in contrast to those realized by zero modes confined to vortices or interfaces between phases. This difference is reflected in the way of measuring the fusion outcome of two anyons. For a pair of zero modes at two ends of a superconducting wire, the outcome can be measured by interfering a vortex around the superconductor and then measuring the phase shift induced by the Aharonov-Casher effect (*53*). In contrast, for the FQHE anyons, qubit measurements can be carried out by interfering the anyons themselves (*54*–*56*). We note that the unitary transformations required for topological quantum computing can be simulated using only measurements of fusion outcomes (instead of performing braiding operations) (*57*).

Outlook

The field of topological quantum computation is in its infancy. On the experimental side, there has been substantial recent progress in the study of systems that host Majorana fermions. So far, this study has mostly attempted to demonstrate the existence of these Majorana fermions. In the near future, one may expect further experiments aimed at nailing down the identification of these systems as non-Abelian, together with the development of methods to control, manipulate, and braid the anyons. Concurrently, one may expect experimental attempts to form hybrids of topological and nontopological qubits. These experiments will surely benefit from detailed theoretical modeling of the experimental systems. Future theoretical studies will hopefully propose novel non-Abelian systems that could be realized experimentally. These studies will benefit from an ongoing effort to classify non-Abelian states and explore the underlying mathematical structures. On the quantum computer science front, much remains to be understood regarding the computational power of various types of non-Abelian systems. Future studies may refine the distinction between universal and nonuniversal quantum computation, and distinguish between more and less powerful schemes for nonuniversal quantum computation.

References and Notes

1. G. Moore, N. Read, *Nucl. Phys. B* **360**, 362 (1991).
2. C. Nayak, S. H. Simon, A. Stern, M. Freedman, S. Das Sarma, *Rev. Mod. Phys.* **80**, 1083 (2008), and references therein.
3. A. Yu. Kitaev, *Ann. Phys.* **303**, 2 (2003).
4. M. H. Freedman, M. Larsen, Z. Wang, *Comm. Math. Phys.* **227**, 605 (2002).
5. M. Freedman, C. Nayak, K. Walker, *Phys. Rev. B* **73**, 245307 (2006).
6. J. Preskill, Lecture Notes on Quantum Computation (www.theory.caltech.edu/~preskill/ph219/topological.pdf).
7. A. Stern, *Nature* **464**, 187 (2010).
8. J. Alicea, *Rep. Prog. Phys.* **75**, 076501 (2012).
9. A. Kitaev, *Ann. Phys.* **321**, 2 (2006).
10. C. Nayak, F. Wilczek, *Nucl. Phys. B* **479**, 529 (1996).
11. The degeneracy of the ground state is never perfect. The energy splitting between the different ground states is exponentially small in the ratio of the anyons' separation and a (system-dependent) microscopic length scale. It can thus be made arbitrarily small by increasing this separation.
12. A. Yu. Kitaev, *Russ. Math. Surv.* **52**, 1191 (1997).
13. M. A. Nielsen, I. L. Chuang, *Quantum Computation and Quantum Information* (Cambridge Univ. Press, Cambridge, 2000).
14. S. Bravyi, A. Yu. Kitaev, *Phys. Rev. A* **71**, 022316 (2005).
15. S. Bravyi, *Phys. Rev. A* **73**, 042313 (2006).
16. N. Read, D. Green, *Phys. Rev. B* **61**, 10267 (2000).
17. A. Yu. Kitaev, *Phys. Uspekhi* **44** (suppl. 10), 131 (2001).
18. D. A. Ivanov, *Phys. Rev. Lett.* **86**, 268 (2001).
19. A. Stern, F. von Oppen, E. Mariani, *Phys. Rev. B* **70**, 205338 (2004).
20. J. Alicea, Y. Oreg, G. Refael, F. von Oppen, M. P. A. Fisher, *Nat. Phys.* **7**, 412 (2011).
21. B. I. Halperin *et al.*, *Phys. Rev. B* **85**, 144501 (2012).
22. J. D. Sau, D. J. Clarke, S. Tewari, *Phys. Rev. B* **84**, 094505 (2011).
23. L. Fu, C. L. Kane, *Phys. Rev. Lett.* **100**, 096407 (2008).
24. L. Fu, C. L. Kane, *Phys. Rev. B* **79**, 161408 (2009).
25. J. D. Sau, R. M. Lutchyn, S. Tewari, S. Das Sarma, *Phys. Rev. Lett.* **104**, 040502 (2010).
26. R. M. Lutchyn, J. D. Sau, S. Das Sarma, *Phys. Rev. Lett.* **105**, 077001 (2010).
27. Y. Oreg, G. Refael, F. von Oppen, *Phys. Rev. Lett.* **105**, 177002 (2010).
28. V. Mourik *et al.*, *Science* **336**, 1003 (2012).
29. A. Das *et al.*, *Nat. Phys.* **8**, 887 (2012).
30. A. D. K. Finck, D. J. Van Harlingen, P. K. Mohseni, X. Li, K. Jung, http://arXiv.org/abs/1212.1101 (2012).
31. L. P. Rokhinson, X. Liu, J. K. Furdyna, *Nat. Phys.* **8**, 795 (2012).
32. M. T. Deng *et al.*, *Nano Lett.* **12**, 6414 (2012).
33. D. Gottesman, http://arxiv.org/abs/quant-ph/9705052 (1997).
34. G. Duclos-Cianci, K. M. Svore, http://arXiv.org/abs/1210.1980 (2012).
35. E. Dennis, A. Yu. Kitaev, A. Landahl, J. Preskill, *J. Math. Phys.* **43**, 4452 (2002).
36. F. Hassler, A. R. Akhmerov, C.-Y. Hou, C. W. J. Beenakker, *N. J. Phys.* **12**, 125002 (2010).
37. P. Bonderson, D. J. Clarke, C. Nayak, K. Shtengel, *Phys. Rev. Lett.* **104**, 180505 (2010).
38. E. Grosfeld, A. Stern, *Proc. Natl. Acad. Sci. U.S.A.* **108**, 11810 (2011).
39. L. Jiang, C. L. Kane, J. Preskill, *Phys. Rev. Lett.* **106**, 130504 (2011).
40. P. Bonderson, R. M. Lutchyn, *Phys. Rev. Lett.* **106**, 130505 (2011).
41. F. Hassler, A. R. Akhmerov, C. W. J. Beenakker, *N. J. Phys.* **13**, 095004 (2011).
42. N. H. Lindner, E. Berg, G. Refael, A. Stern, *Phys. Rev. X* **2**, 041002 (2012).
43. D. J. Clarke, J. Alicea, K. Shtengel, *Nat. Commun.* **4**, 1348 (2013).
44. M. Cheng, *Phys. Rev. B* **86**, 195126 (2012).
45. A. Vaezi, *Phys. Rev. B* **87**, 035132 (2013).
46. M. Barkeshli, C.-M. Jian, X.-L. Qi, *Phys. Rev. B* **87**, 045130 (2013).
47. M. B. Hastings, C. Nayak, Z. Wang, http://arXiv.org/abs/1210.5477 (2012).
48. N. Read, E. Rezayi, *Phys. Rev. B* **54**, 16864 (1996).
49. M. Storni, R. H. Morf, S. Das Sarma, *Phys. Rev. Lett.* **104**, 076803 (2010).
50. R. L. Willett, L. N. Pfeiffer, K. W. West, *Phys. Rev. B* **82**, 205301 (2010).
51. A. Bid *et al.*, *Nature* **466**, 585 (2010).
52. S. An *et al.*, http://arXiv.org/abs/1112.3400 (2011).
53. Y. Aharonov, A. Casher, *Phys. Rev. Lett.* **53**, 319 (1984).
54. S. Das Sarma, M. Freedman, C. Nayak, *Phys. Rev. Lett.* **94**, 166802 (2005).
55. A. Stern, B. I. Halperin, *Phys. Rev. Lett.* **96**, 016802 (2006).
56. P. Bonderson, A. Kitaev, K. Shtengel, *Phys. Rev. Lett.* **96**, 016803 (2006).
57. P. Bonderson, M. Freedman, C. Nayak, *Ann. Phys.* **324**, 787 (2009).
58. R. L. Willett, C. Nayak, K. Shtengel, L. N. Pfeiffer, K. W. West, http://arXiv.org/abs/1301.2639 (2013).

Acknowledgments: We thank C. Nayak and J. Preskill for helpful discussions, and the Kavli Institute for Theoretical Physics for their hospitality. Supported by the U.S.-Israel Binational Science Foundation, the Minerva foundation, and Microsoft Station Q (A.S.); Defense Advanced Research Projects Agency award N66001-12-1-4034 and the Institute for Quantum Information and Matter, an NSF Physics Frontiers Center, with support of the Gordon and Betty Moore Foundation (N.H.L.); and NSF grant PHY11-25915.

10.1126/science.1231473